

CRACOW UNIVERSITY OF TECHNOLOGY
Faculty of Applied Physics
Institute of Physics, Mathematics and Informatics



IGOR SKIBA

Nº of student's book: 97740
Degree course: Applied Physics

Master Thesis Full Time Studies

Infrared Researching of PbSe/PbSrSe Multiple Quantum Wells Semiconductor Structures

**Badanie Wielokrotnych Studni Kwantowych Struktur Półprzewodnikowych
PbSe/PbSrSe w Podczerwieni**

Mark:
Promotor signature:.....
Promotor: **Prof. dr hab. Tadeusz Lesiak**

Cracow, May 2017

Acknowledgments

I would like to express my deep gratitude to:

my supervisor, prof. dr hab. Tadeusz Lesiak
for patience, kindness and valuable feedback
during creation of this master thesis.

I would like to thank also
Camlin Technologies Switzerland team
for enabling me doing research during my
internship necessary for this master thesis.

I would like to thank sincerely in particular:
dr. Alfonso Gonzalez Taboada
for leading me into the exciting research field of
semiconductor optics and
quantum mechanics as well as guiding,
supporting and helping me during the creation
of this master thesis.

Last but not least, I would like to give my
thanks to my parents
Alicja and Wojciech
for constant support and love - I would not be
where I am now if it were not for You.

Author.

ABSTRACT

The main purpose of this master thesis was to elaborate the study of PbSe/PbSrSe semiconductor materials with multiple number of quantum wells system grown on top of Si (111) in infrared. The work includes the general information about IV-VI semiconductors, quantum mechanics of semiconductors and photoluminescence spectroscopy. Experimental set-up as well as obtained results and conclusions were discussed thoroughly.

Głównym celem tej pracy magisterskiej było przestudiowanie oraz przedyskutowanie materiałów półprzewodnikowych PbSe/PbSrSe z systemami wielokrotnych studni kwantowych wyprodukowanych na górnej powierzchni Si (111) w podczerwieni. Praca zawiera podstawowe informacje na temat półprzewodników IV-VI, mechanice kwantowej półprzewodników oraz spektroskopii fotoluminesencyjnej. Eksperymentalny układ pomiarowy, jak również otrzymane wyniki i konkluzje zostały dokładnie przedyskutowane.

Table of Contents

Subject and Aim of Thesis.....	7
Scope of Work	7
I. Theoretical Introduction	8
1. IV-VI Semiconductors	8
1.1. Material Properties	8
1.2. Structural Properties.....	9
1.3. Electronic Properties	9
1.4. Optical Properties	9
1.5. Application	9
2. Infrared.....	10
3. Quantum Semiconductor Mechanics.....	11
3.1. Types of Low-Dimensional Semiconductors	11
3.2. Density of States in Low-Dimensional Semiconductors.....	12
3.3. Quantum Well.....	15
3.3.1. Quantum Well with Infinite Barriers	15
3.3.2. Quantum Well with Finite Barriers	17
4. Photoluminescence Spectroscopy	21
4.1. Recombinations	21
4.1.1. Spontaneous Recombination.....	21
4.1.2. Stimulated Generation	22
4.1.3. Stimulated Recombination	22
4.1.4. Non-Radiative Recombination.....	22
4.2. Epitaxial Growth Technology.....	23
II. Experimental Set-up Part	24
5. Experimental Set-up	24
5.1. Sample.....	24
5.1.1. Sample Cleanliness and Mounting.....	25
5.2. Alignment.....	26
5.3. FTIR (Fourier Transform Infrared) Spectrometer.....	27
5.4. Nomarsky Microscope	28
5.5. Pumps	29
5.6. Lock-In Amplifier and Chopper.....	29
5.7. Oscilloscope	30
5.8. Detector.....	31
5.9. Temperature Controls	31
5.10. Laser	32
III. Research Part.....	33
6. Photoluminescence of PbSe/PbSrSe Semiconductor Materials in IR	33
6.1. Set-up Reliability Check.....	33
6.2. Number of Quantum Wells	38
6.3. Sr Content.....	43
7. Conclusions and Final Remarks	50
8. Bibliography	51

Subject and Aim of Thesis

The aim of the present master thesis work was to study and investigate specific IV-VI semiconductor materials, namely PbSe/PbSrSe. On the basis of performed measurements on very different set of samples, conclusions were drawn. The work had also a purpose to broaden horizons about electronics, opto-electronics and quantum mechanics.

Scope of Work

The scope of work has been divided into three major parts: the theoretical part, the experimental set-up part and the research one. The theoretical part gives a short introduction about infrared and semiconductors which have been used to measure photoluminescence. The basic concepts of quantum mechanics have been covered to understand the mechanics of quantum wells. Lastly, the photoluminescence effect has been explained. As for the experimental set-up part, all the components of the optic set-up have been discussed in details. The third chapter concerns the acquired data of performed measurements, graphs and conclusions.

I. Theoretical Introduction

Semiconductors revolutionized the world we live in. The life as we know would be completely different if not for these materials. They are present in almost every electrical machines and devices, and so there is a constant pursuit to make them more efficient and productive. In Camlin Technologies Switzerland company, researches are being performed to achieve a continuous wave operation in mid-IR (mid-infrared) with the development of VECSEL (Vertical External Cavity Surface Emitting Laser) which is based on IV-VI semiconductors covering wavelengths from $3.0\mu\text{m}$ to $4.5\mu\text{m}$.

1. IV-VI Semiconductors

Semiconductors are made up from different elements hence their properties vary. However, they share certain similarities. Properties of semiconductors are related to their atomic characteristics. A semiconductor can take many forms, from a single element (Si), a compound (GaAs) to an alloy ($\text{Si}_x\text{Ge}_{(1-x)}$).

Let us consider IV-VI semiconductor compounds. They are formed by elements in group IV (Ge, Sn and Pb) and VI (S, Se, Te) of the periodic table. They are regarded as oldest semiconductor materials. The most leading representatives are PbS, PbSe and PbTe which have been used successfully for over a century for electronic and optoelectronic devices in mid-IR (mid-infrared) and not only.

1.1. Material Properties

In comparison to most widely used semiconductors such as Si and Ge, III-V (GaAs, InAs, AlAs) and II-VI (ZnTe, CdTe), IV-VI semiconductors have ten bonding electrons per atom pair instead of eight. Individual atoms are bonded together in a regular periodic structure – 6 electrons per atom pair supports a hybridization with the bond orbitals at the angle of 90° with respect to each other resulting in a 6-fold coordination of the atoms in the lattice, as opposed to the 4-fold coordination of the most common semiconductors. Such arrangement causes differences between III-V, II-VI semiconductors and IV-VI semiconductors in terms of the crystal structure, physical and electronic properties. The other significant factor of IV-VI semiconductors is the fact that their bondings are not entirely covalent – they exhibit also ionic and metallic bonding.

1.2. Structural Properties

Even though IV-VI compounds are 6-fold coordinated, the differences in covalent, ionic and metallic bonding contribution cause polymorphism meaning that crystallization occurs in different crystal structures. Because of their crystalline quality which does not degrade with repeatable thermal cycling as well as good plasticity (working well in tension and in compression) they are used in fabrication of reliable lasers on silicon-based substrates.

1.3. Electronic Properties

IV-VI compounds (mainly PbSe and PbTe) are characterized by a narrow direct energy gap between the valence and the conduction band. This favors absorption and emission of photons on the edges of the band making them efficient in optoelectronics as photon detector or photon emitter devices. The energy band gap of the lead salt compounds (PbSe and PbS) decreases while the temperature decreases resulting in a huge change with respect to the absolute value of the band gap. This finds its usage in spectroscopy at mid-IR lasers, allowing simple tuning of the emission wavelength over a broad range. Additionally, lead salt compounds possess a high static dielectric constant with values greater than hundred. This is caused because these compounds are near to a structural phase transition from the cubic structure to the rhombohedral one which grants ferroelectric properties. In comparison to other semiconductor materials, the conduction and valence bands are almost symmetrical causing a high mobility of electrons and holes which enhance transportation properties. But high dielectric constants also boost electron-hole mobilities because they effect screening of charged impurities. At low temperatures, the mobility is mainly defined by ionized impurity scattering.

1.4. Optical Properties

Because of the extraordinary narrow band structure of lead salts compounds which results in high values of the absorption constants leads to strong absorption of photons with energies greater than fundamental energy gap. These aspect makes them superior than their cousins III-V or II-VI semiconductors in terms of optics.

1.5. Application

Discussed properties of IV-VI semiconductors distinguish them on semiconductor's scene in opto-electronics in mid-IR as mentioned before. Nevertheless, the application is much greater. They find its use in IR detectors in medical breath diagnosis. A breath exhaled by a patient is quickly analyzed and so respiratory diseases may be detected like asthma. They are used also in thermoelectrics (thermoelectric coolers) and telecommunication while they are also manufacture as temperature sensors, holographic recording systems and memory switching devices. Moreover, they can be used to monitor industrial processes gases and air pollutants.

2. Infrared

Because of the wave-particle duality nature of light, electromagnetic radiations can be considered as waves or particles at different wavelengths and frequencies. The range of wavelengths is called the electromagnetic spectrum which is divided into seven regions: gamma rays, x-rays, ultraviolet, visible light, infrared, microwave and radio waves.

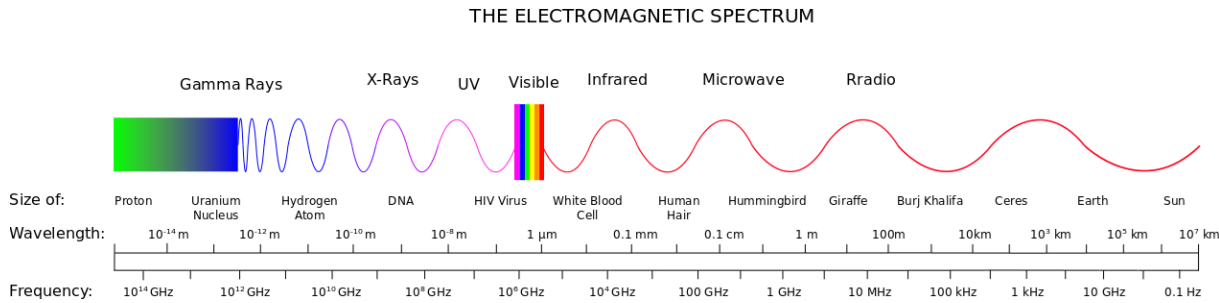


Fig. 2.1. The electromagnetic spectrum.

Infrared (IR) is a type of electromagnetic radiation with the wavelength longer than visible light, although the boundary between IR and visible light is not precisely defined. IR is also referred as “heat radiation” because of being one of three heat transfer forms. Other two are conduction and convection. Every object of higher temperature than $\sim 5\text{K}$ emits IR radiation.

Mid infrared division:

- Near-infrared
- Short-wavelength infrared
- Mid-wavelength infrared
- Long-wavelength infrared
- Far-infrared

Abbrev.:

NIR	$\sim 0.7\mu\text{m} - 1.4\mu\text{m}$
SWIR	$1.4\mu\text{m} - 3\mu\text{m}$
MIR	$3\mu\text{m} - 8\mu\text{m}$
LWIR	$8\mu\text{m} - 15\mu\text{m}$
FIR	$15\mu\text{m} - 1000\mu\text{m}$

Range:

IR found its application in identification and analysis of substances. This, called IR spectroscopy, measures IR emissions of materials at certain wavelengths.

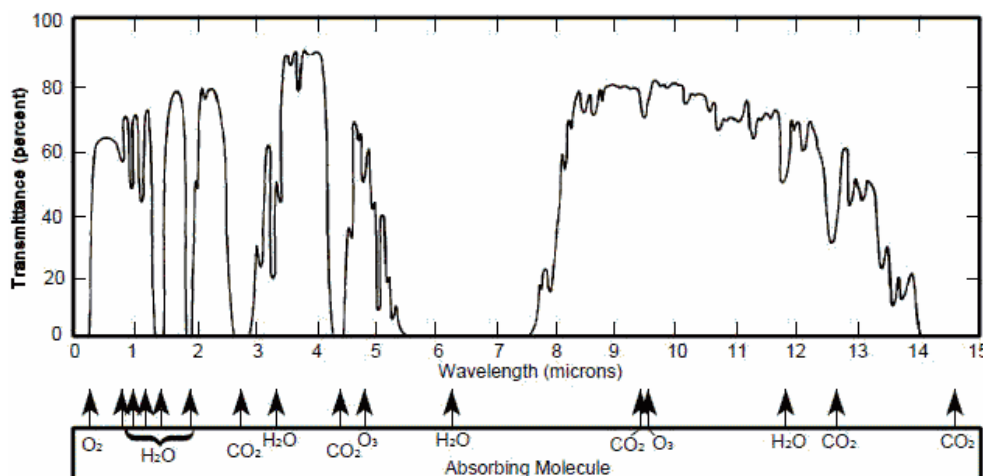


Fig. 2.2. Infrared spectrum.

3. Quantum Semiconductor Mechanics

When the size of a material drops below 100nm, certain properties cannot be described in classical physics. Such nanostructures are explained through quantum mechanics. Quantum mechanics is a primary branch of physics explaining the behavior of matter and interactions with energy of sizes of atoms and subatomic particles.

3.1. Types of Low-Dimensional Semiconductors

Low-dimensional semiconductors are divided because of their confinement in particular directions. Quantum confinement takes place when diameter of a material is of the same magnitude as the de Broglie wavelength of the electron wave function producing new material behavior, changing their optical and electronic properties.

Depending on the dimensionality, the following classification occurs:

- bulk crystal – no confinement of a particle motion occurs. A particle can move in every three dimensions.
- quantum well – a particle is confined in one dimension,
- quantum wire – a particle is confined in two dimensions,
- quantum dot – extreme case of size reduction, a particle is confined in all three dimensions.

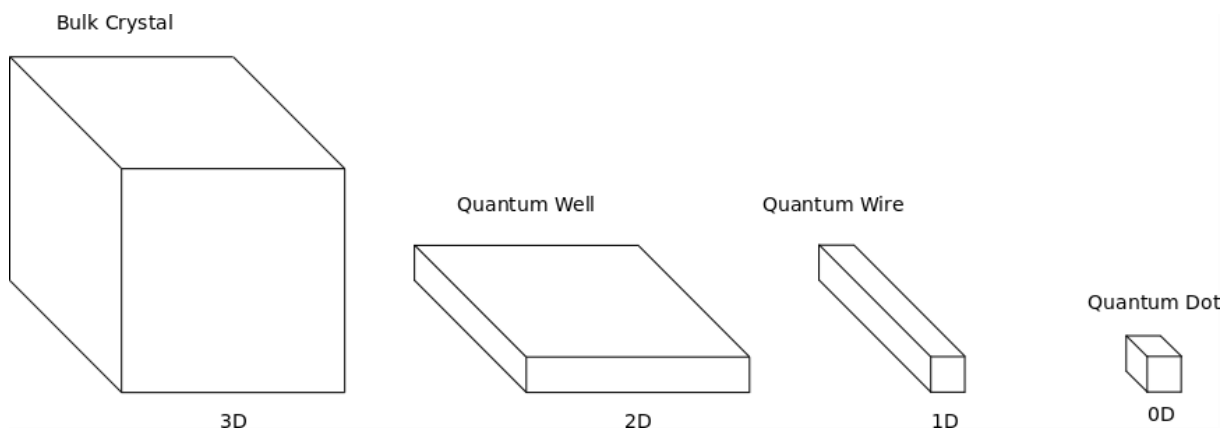


Fig. 3.1. Graphical representation of low-dimensional semiconductors.

Usual size dimensions for quantum well vary between 1mm and 1000nm (thickness), for quantum wire between 1nm and 100nm (radius) whereas for quantum dot it is around 1nm and 10nm (radius).

3.2. Density of States in Low-Dimensional Semiconductors

Density of states is a quantum mechanical function describing the number of accessible states on energy unit that can be occupied by electrons.

The product of quasi-particle wavefunction in the form of plane wave $\phi(r) = Ke^{ikr}$ and its complex conjugate $\phi(r)\phi^*(r)dV = w(r)dV$ yields the probability of finding a particle inside the volume $dV = dx dy dz$ at the position characterized by vector r . Integral of the probability density over entire volume where the particle is located has to be equal to 1.

$$1 = \int w(r)dV = \int \phi(r)\phi^*(r)dV = K^2 \int e^{ikr}e^{-ikr}dV = K^2 V.$$

This equation allows finding the coefficient K .

$$K = \frac{1}{\sqrt{V}},$$

$$\begin{array}{lll} 3D & \rightarrow & V = L^3 \\ 2D & \rightarrow & V = L^2 \\ 1D & \rightarrow & V = L \end{array} \rightarrow \begin{array}{lll} K = L^{-3/2}, \\ K = L^{-1}, \\ K = L^{-1/2}. \end{array}$$

If a quasi-particle is restricted in the x-axis of a segment length L and the barriers are impenetrable meaning that the possibility of finding the particle beyond barriers equals 0, then the wavefunction has to reach 0 at the edge of each barrier. These boundary conditions are satisfied only by standing waves. Standing wave is a wave formed by a superposition of waves with inverse wavevectors $-k$ and k where $|k| = \frac{n\pi}{L}$.

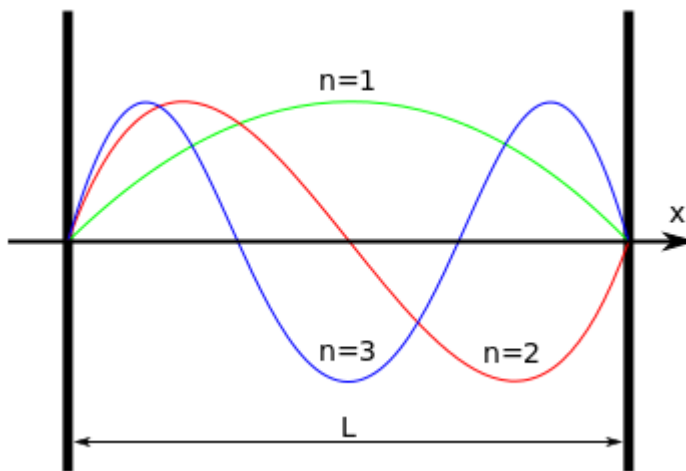


Fig. 3.2. Wavefunctions of a particle confined between barriers.

To calculate density of states $\rho(k)$ in k-space, it is needed to count the number of states within the segments $(k, k + dk)$ and $(-k, -k - dk)$. The number of states is established between the k radius and $k + dk$ (fig. 6.).

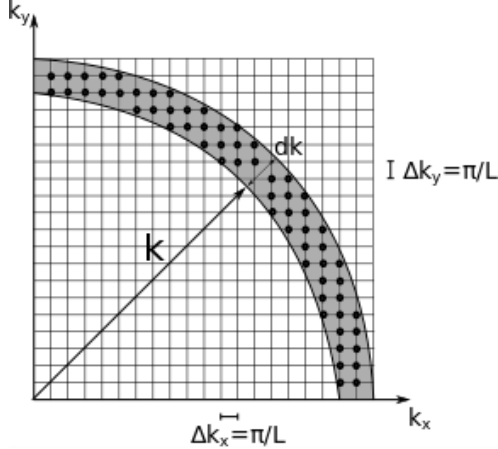


Fig. 3.3. Density of states in two-dimensional k-space.

The density of states $\rho(k)$ equals:

$$\rho(k)dk = g_s V_k \frac{1}{\left(\frac{\pi}{L}\right)^d},$$

where d is the number of dimensions, g_s is the degeneracy factor (equals 2 for fermions) and dV_k is the volume of k -space where the wavevector projections k_x , k_y and k_z are positive and their amplitude k lies in the range of $(k, k + dk)$. The elemental volumes equal:

$$\begin{aligned} 1D &\rightarrow dV_k = \frac{1}{2}dk, \\ 2D &\rightarrow dV_k = \frac{\pi k}{2}dk, \\ 3D &\rightarrow dV_k = \frac{\pi k^2}{2}dk. \end{aligned}$$

By substituting dV_k into the equation of density of states:

$$\begin{aligned} 1D &\rightarrow \rho(k)dk = g_s \frac{L}{2\pi}dk, \\ 2D &\rightarrow \rho(k)dk = g_s \frac{L^2 k}{2\pi}dk, \\ 3D &\rightarrow \rho(k)dk = g_s \frac{L^3 k^2}{2\pi}dk. \end{aligned}$$

To obtain the density of states related to energy (changing k-space into energy-space) the following relation should be used:

$$\rho(E)dE = \rho(k(E)) \frac{dk}{dE} dE.$$

After solving above equation:

$$E(k_h) = -\frac{\hbar^2 k_h^2}{2m_h},$$

$$E(k_e) = E_g + \frac{\hbar^2 k_e^2}{2m_e}.$$

Considering an electron in the conduction band, it is possible to derive the wavevector and its derivative with respect to E . Subscript 'e' has been omitted in order to simplify the equations.

$$k = \frac{\sqrt{2m}}{\hbar} \sqrt{E - E_g},$$

$$\frac{dk}{dE} = \frac{\sqrt{2m}}{\hbar} \frac{1}{\sqrt{E - E_g}}.$$

After combining these two equations with equations determining the density of states and substituting them into energy, the density of states of electrons in the conduction band for specific dimensions are as follows:

$$1D \rightarrow \rho(E)dE = g_s \frac{\sqrt{2m}}{4\pi\hbar} \frac{1}{\sqrt{E - E_g}},$$

$$2D \rightarrow \rho(E)dE = g_s \frac{2m}{4\pi\hbar^2},$$

$$3D \rightarrow \rho(E)dE = g_s \frac{(2m)^{\frac{3}{2}}}{4\pi\hbar^3} \sqrt{E - E_g}.$$

To summarize, the density of states of a hole in the valence band and an electron in the conduction band can be noted as:

$$\rho_c(E) \sim (E - E_g)^{\frac{d}{2-1}} \quad E > E_g,$$

$$\rho_v(E) \sim |E|^{\frac{d}{2-1}} \quad E < 0.$$

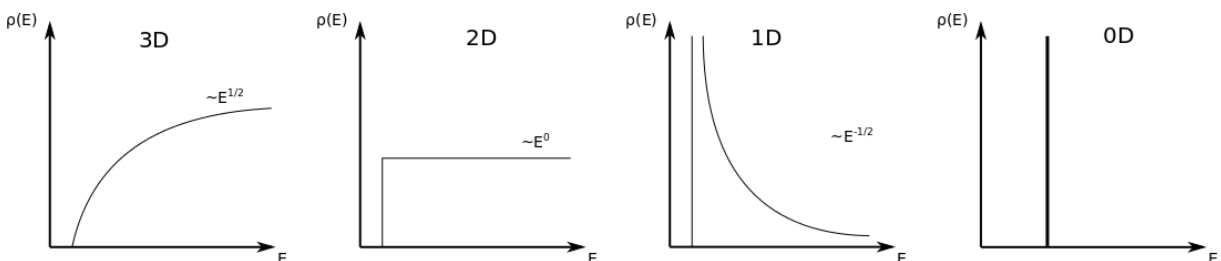


Fig. 3.4. Density of states in the conduction band of specific semiconductor structures.

3.3. Quantum Well

A quantum well is a thin layer which confines particles (electrons and holes) in dimension perpendicular to the layer surface whereas other two dimensions are not restricted allowing free movement of carriers. Generally, a quantum well is a segment of a semiconductor, surrounded by a different semiconductor with a wider bandgap.

3.3.1. Quantum Well with Infinite Barriers

Let us consider two-dimensional system where a free particle is located inside the well. The well is placed symmetrically with respect to the origin of the coordinate system. The potential energy of free particle $V(z)$ inside the well is equal:

$$V(z) = \begin{cases} 0, & -\frac{L_z}{2} < z < \frac{L_z}{2}, \\ \infty, & \infty < z < -\frac{L_z}{2} \wedge \frac{L_z}{2} > z > \infty. \end{cases}$$

The thickness of well L_z gives a finite volume for the particle. The Schrödinger equation for a quasi-particle being confined in the quantum well of $V(z)$ equals:

$$\left[\frac{-\hbar^2}{2m} \nabla^2 + V(z) \right] \psi(x, y, z) = E \psi(x, y, z).$$

To solve this equation, it is recommended to transfer it into two equations. The first equation will consider the motion in perpendicular direction (x-y plane) to confinement where there is no restriction in movement. The second part will describe the movement in the parallel direction (z plane) where the confinement takes place. To achieve that, the Laplace operator, wavefunction and energy eigenvalues have to be separated.

$$\begin{aligned} \nabla^2 &= \frac{\partial^2}{\partial x^2} + \frac{\partial^2}{\partial y^2} + \frac{\partial^2}{\partial z^2} = \nabla_{\perp}^2 + \frac{\partial^2}{\partial z^2}, \\ \psi(x, y, z) &= \phi(x, y) \zeta(z), \\ E &= E_{\perp} + E_z. \end{aligned}$$

Plane x-y is denoted as \perp . Now, it is possible to rewrite the original equation:

$$\begin{aligned} \frac{-\hbar^2}{2m} \nabla_{\perp}^2 \phi(x, y) &= E_{\perp} \phi(x, y), \\ \left[\frac{-\hbar^2}{2m} \frac{\partial^2}{\partial z^2} + V(z) \right] \zeta(z) &= E_z \zeta(z). \end{aligned}$$

Let us focus on the first equation which describes the free motion inside x-y plane. The dispersion relation takes the form of parabolic bands:

$$E_{\perp} = \frac{\hbar^2}{2m} (k_x^2 + k_y^2) = \frac{\hbar^2}{2m} k_{\perp}^2.$$

Hence, the electrons and holes are described as follows:

$$E_e(k) = E_g + \frac{\hbar^2}{2m_e} (k_x^2 + k_y^2),$$

$$E_h(k) = -\frac{\hbar^2}{2m_h} (k_x^2 + k_y^2).$$

Now, it is time to consider the second equation which describes the motion in the direction perpendicular to the layer.

$$\left[-\frac{\hbar^2}{2m} \frac{\partial^2}{\partial z^2} + V(z) \right] \zeta(z) = E_z \zeta(z).$$

Because there is no possibility for the particle to escape through infinite walls (the probability of finding the particle beyond the well boundaries equals 0) let us look for the wavefunction inside the well where $V(z) = 0$.

$$-\frac{\hbar^2}{2m} \frac{\partial^2}{\partial z^2} \zeta(z) = E_z \zeta(z),$$

let $k_z^2 = \frac{2mE}{\hbar^2}$, then:

$$\frac{\partial^2 \zeta(z)}{\partial z^2} + k_z^2 \zeta(z) = 0.$$

Above right-sided equation can be treated as the equation of a harmonic oscillator and so the solution is well known.

$$\zeta(z) = A \sin(k_z z) + B \cos(k_z z).$$

Boundary conditions have to be fulfilled which means that at the edges of well the wavefunction has to be equal to 0. Because the well is symmetrical, the solution might be even or odd:

$$\zeta^+(z) = B \cos(k_z z),$$

$$\zeta^-(z) = A \sin(k_z z).$$

The normalization condition allows determination of coefficients A and B .

$$\langle \zeta(z) | \zeta(z) \rangle = 1 \quad \rightarrow \quad A = B = \sqrt{\frac{2}{L_z}}.$$

The boundary conditions specify the allowed values of the wavevectors.

$$\sqrt{\frac{2}{L_z}} \cos\left(\frac{k_z^+ L_z}{2}\right) = 0 \quad \rightarrow \quad \frac{k_z^+ L_z}{2} = \left(j_e - \frac{1}{2}\right)\pi, \quad j_e = 1, 2, 3, \dots,$$

$$\sqrt{\frac{2}{L_z}} \sin\left(\frac{k_z^+ L_z}{2}\right) = 0 \quad \rightarrow \quad \frac{k_z^+ L_z}{2} = j_o \pi, \quad j_e = 1, 2, 3, \dots$$

Using two equations separated at the beginning of this chapter, the following wavefunctions and the corresponding energies are able to be determined.

$$\begin{aligned}\zeta^+(z) &= \sqrt{\frac{2}{L_z}} \cos\left(\frac{2\pi(j_e - \frac{1}{2})}{L_z} z\right), \quad j_e = 1, 2, 3, \dots, \\ E_z^+ &= \frac{2\left(j_e - \frac{1}{2}\right)^2 \hbar^2 \pi^2}{2mL_z^2}, \quad j_e = 1, 2, 3, \dots, \\ \zeta^-(z) &= \sqrt{\frac{2}{L_z}} \sin\left(\frac{2\pi j_o}{L_z} z\right), \quad j_e = 1, 2, 3, \dots, \\ E_z^- &= \frac{4j_o^2 \hbar^2 \pi^2}{2mL_z^2}, \quad j_e = 1, 2, 3, \dots\end{aligned}$$

A quasi-particle inside a well with the lowest possible energy (ground state) takes result of the first even solution. The next state (excited state) corresponds to the first odd solution, the next higher state corresponds to the second even solution and so on.

Total energy of a quasi-particle inside a well with infinitely high walls is the sum of partial energies.

$$E = E_{\perp} + E_z = \frac{\hbar^2}{2m} \left(\frac{j^2 \pi^2}{L_z^2} + k_{\perp}^2 \right), \quad j = 1, 2, 3, \dots,$$

where j is a quantum number.

3.3.2. Quantum Well with finite Barriers

Let us consider not a theoretical but a real quantum well with finite height. The crucial difference between the previous example of a quantum well with infinite height is the fact, that now there is a possibility of finding a particle beyond a well. Inside a quantum well, the solution does not really change comparing to the previous example.

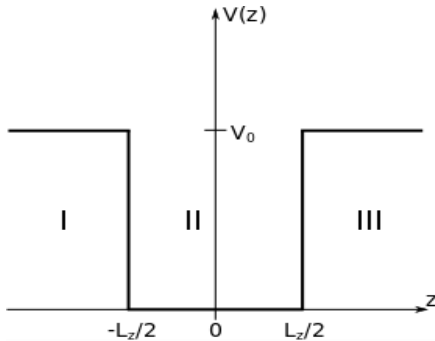


Fig. 3.5. Sketch of a quantum well with finite barriers.

The potential energy of a free particle $V(z)$ equals:

$$V(z) = \begin{cases} 0, & \frac{-L_z}{2} < z < \frac{L_z}{2}, \\ \infty, & \infty < z < \frac{-L_z}{2} \wedge \frac{L_z}{2} > z > \infty. \end{cases}$$

The following system depicted in the fig.8 shows three distinctive regions. Regions I and III hold the equation:

$$\frac{\partial^2 \zeta(z)}{\partial z^2} - \frac{2m}{\hbar^2} (V_0 - E_\lambda) \zeta(z) = 0.$$

Let $\frac{2m}{\hbar^2} (V_0 - E_\lambda) = K_z^2$. Then:

$$\frac{\partial^2 \zeta(z)}{\partial z^2} - K_z^2 \zeta(z) = 0.$$

The solution takes the form:

$$\zeta(z) = C e^{+K_z z} + D e^{-K_z z},$$

however, for the first region when $x \rightarrow \infty$, $D = 0$ and for the third region when $x \rightarrow -\infty$, $C = 0$. And so, the solutions are as follow:

region I:	$\zeta(z) = C e^{+K_z z}$
region III:	$\zeta(z) = D e^{-K_z z}$

Region II is the same example as shown in the previous chapter. To remind it briefly:

$$\frac{\partial^2 \zeta(z)}{\partial z^2} + \frac{2m}{\hbar^2} E_z \zeta(z) = 0,$$

with $k_z^2 = \frac{2mE}{\hbar^2}$:

$$\frac{\partial^2 \zeta(z)}{\partial z^2} + k_z^2 \zeta(z) = 0,$$

and its solution:

region II:	$\zeta(z) = A \sin(k_z z) + B \cos(k_z z).$
------------	---

For even states, this condition gives $A = 0$ and $C = D$, whereas for odd states it gives $B = 0$ and $C = -D$. Furthermore, the boundary conditions have to meet continuity of the wavefunctions at the edges of a well. This holds as well for their first derivatives.

$$B \cos\left(k_z^+ \frac{L_z}{2}\right) = C e^{-K_z^+ \frac{L_z}{2}},$$

$$-k_z^+ B \sin\left(k_z^+ \frac{L_z}{2}\right) = -K_z^+ C e^{-K_z^+ \frac{L_z}{2}}.$$

To simplify this set of equations, it is advisable to divide the second equation by the first one and multiply the result by -1 .

$$k_z^+ \tan\left(k_z^+ \frac{L_z}{2}\right) = K_z^+.$$

Substituting $k_z^+ = \sqrt{\frac{2mE_z^+}{\hbar^2}}$ and $K_z^+ = \sqrt{\frac{2m(V_0 - E_z^+)}{\hbar^2}}$, the equation can be written as:

$$\sqrt{E_z^+} \tan\left(\sqrt{\frac{mE_z^+}{2\hbar^2}} L_z\right) = \sqrt{(V_0 - E_z^+)}.$$

After introducing dimensionless variables θ and θ_0 :

$$\theta = \sqrt{\frac{mE_z^+}{2\hbar^2}} L_z,$$

$$\theta_0 = \sqrt{\frac{mV_0}{2\hbar^2}} L_z,$$

for the even states, the equation takes the form:

$$\tan(\theta) = \sqrt{\frac{\theta_0^2}{\theta^2} - 1}.$$

The same goes for odd states:

$$-\sqrt{E_z^-} \cotan\left(\sqrt{\frac{mE_z^-}{2\hbar^2}} L_z\right) = \sqrt{(V_0 - E_z^-)},$$

$$-\cotan(\theta) = \sqrt{\frac{\theta_0^2}{\theta^2} - 1}.$$

The depth of well has to be equal or larger than:

$$V_0 \geq \frac{\pi^2 \hbar^2}{2mL_z^2}.$$

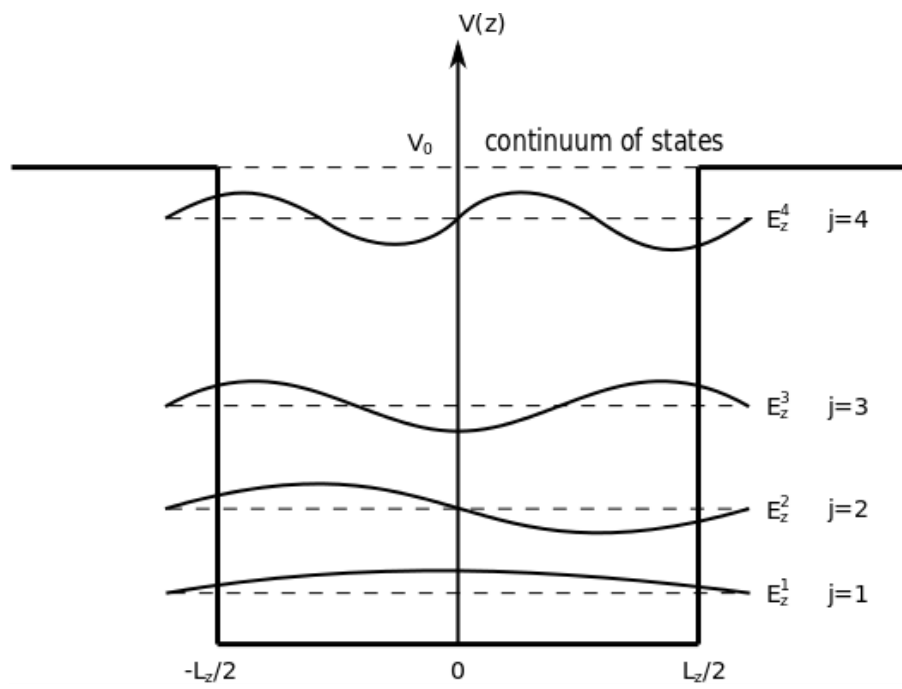


Fig. 3.6. Graphical representation of first four states for a finite well.

4. Photoluminescence Spectroscopy

Photoluminescence (PL) spectroscopy is a powerful and nondestructive method used to investigate electrical and optical characteristics of semiconductor materials, namely carriers' lifetime, band structures, luminescence of impurities as well as quantum properties like: quantum wells, quantum wires and quantum dots. PL can be used a strong non-contact spectroscopy tool widely applied for both scientific research and customary examination of material quality in the semiconductor industry. It consists of the optical excitation of a material to create electron-hole pairs that may form a quasi-particle called exciton. The lifetime of the excitons depends on the crystal lattice, impurity concentration, lattice temperature and dislocation density. The radiative relaxation of such quasiparticles leads to a luminescent response of the photo-excited material called PL. This technique has been reported as a valuable characterization tool for materials commonly used for mid- and long-wavelength IR detection applications.

4.1. Recombinations

- | | | |
|--------------------------------|---|-----------------------------|
| 1. Spontaneous recombination | - | emission of photon |
| 2. Stimulated generation | - | absorption of photon |
| 3. Stimulated recombination | - | coherent emission of photon |
| 4. Non-radiative recombination | - | no emission of photon |

4.1.1. Spontaneous recombination

In semiconductors, electrons and holes can meet spontaneously. Then the recombination process occurs. An electron in the conduction band recombines with a hole in the valence band, an electron falls down and fills a hole (Fig. 10). The excess energy results in creation of a photon. At low temperatures like room temperatures, the accumulation of electrons-holes is too low to acquire sufficient number of spontaneous recombinations. And even if a relatively high number of these events occur, then an incoherent emission would take place because the recombination process would happen randomly (random intervals and directions). However, if electrons feedback is provided (e.g. electrically), then the concentration of electron-hole pairs is significantly increased and so their recombination processes, thus emission of photons can be observed. This is a fundamental mechanism in Light Emitting Diode (LED).

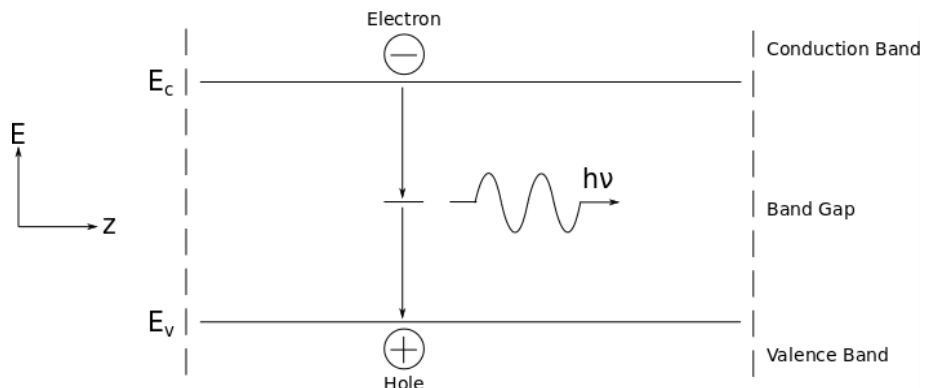


Fig. 4.1. Sketch of spontaneous recombination process.

4.1.2. Stimulated generation

A photon absorption stimulates the formation of an electron in the conduction band and its opposite hole in the valence band.

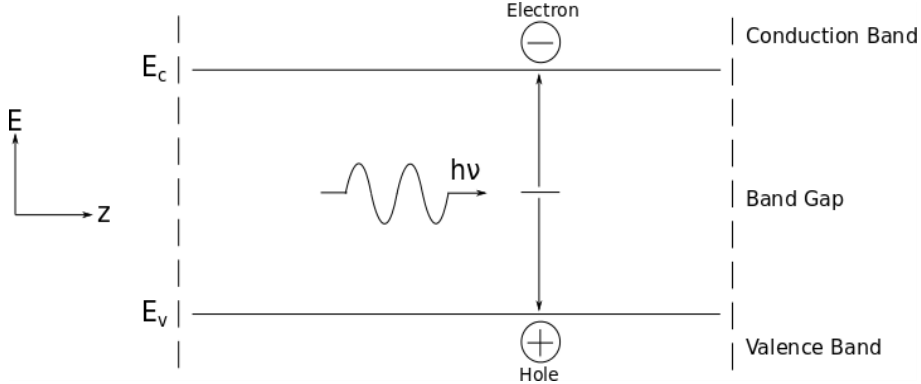


Fig. 4.2. Sketch of stimulated generation process.

4.1.3. Stimulated recombination

An incident photon stimulates the recombination of an electron and a hole and simultaneously creates a new photon. In contrary to the stimulated generation where a photon is absorbed, here a photon fulfils the role of a trigger of this process generating a new photon with the same exact frequency, phase, polarization and direction as the incident photon. This process is a primary mechanism for lasers to generate light as well as fluorescence and thermal emission.

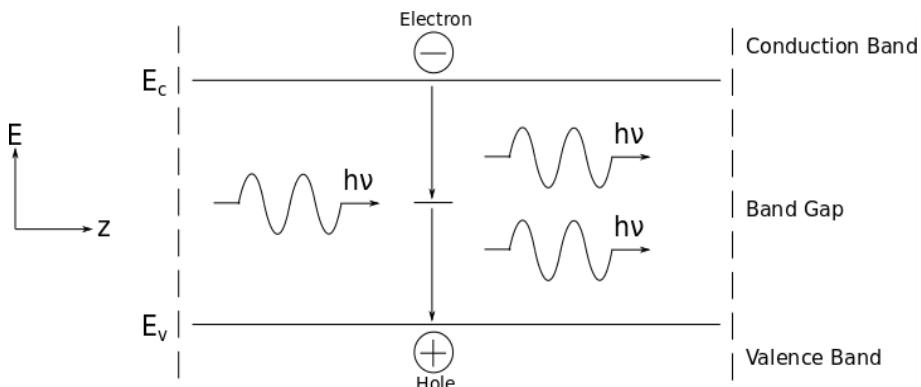


Fig. 4.3. Sketch of stimulated recombination process.

4.1.4. Non-radiative recombination

In non-radiative recombination, an electron from conduction band can recombine with a hole from valence band without generating any photons. In this case energy dissipates as heat in semiconductor crystal lattice. This scenario is not favorable because no photons are created.

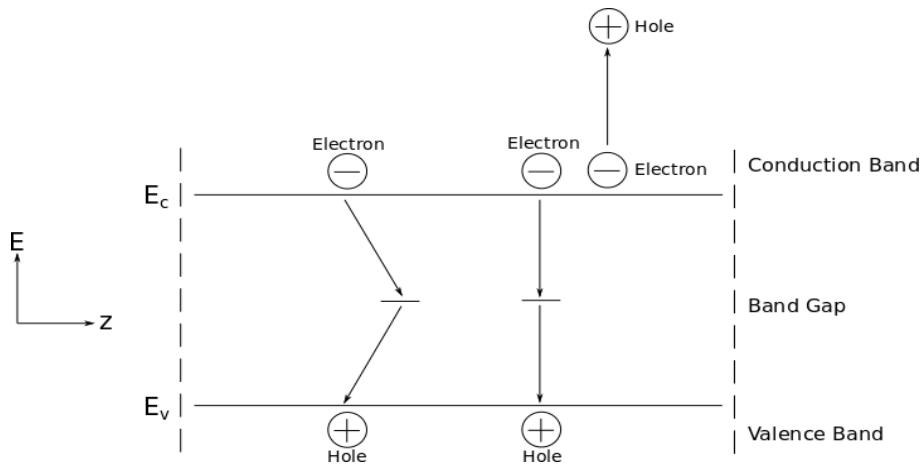


Fig. 4.4. Sketch of non-radiative recombination process.

4.2. Epitaxial Growth Technology

Epitaxy is used in semiconductor industry to achieve multilayer structure essential for diode lasers. It is vital to grow single-crystal lattice-matched layers with exactly controlled thickness over a suitable substrate.

There are three most common techniques:

- LPE (Liquid-Phase Epitaxy)
- MBE (Molecular Beam Epitaxy)
- OMVPE (Organometallic Vapour-Phase Epitaxy)

These three growth methods take place in liquid, vacuum and gas respectively. The general differences between them are as follow:

- In LPE a source material is melted on solid substrate at temperatures below the melting point of the deposited semiconductor.
- In MBE a source material is heated to form an evaporated beam of particles which travel in a high vacuum (10^{-8} Pa) to the substrate where they deposit. This technique is commonly used to grow semiconductor crystals of III, IV and V group.
- In OMVPE in comparison to MBE, the growth is done by chemical reaction rather than physical deposition. This process occurs not in a vacuum but in a gas phase at pressure from 10^3 Pa to 10^5 Pa .

II. Experimental Set-up Part

The main research line of the Camlin Technologies Zürich location (CTCH) faces the development and production of mid-infrared VECSEL with an active layer based on IV-VI semiconductor heterostructures, in particular PbSe/PbSrSe Quantum Wells (QWs). These heterostructures luminesce in a region of the spectrum where ordinary blackbody radiation contributes large amounts of power, thus there is an obstacle of extracting the PL signals from a potentially overwhelming thermal background.

In order to extract the PL signal from the dominant thermal background, the mechanical chopper/lock-in amplifier combination is adapted, traditional in spectroscopic experiments with conventional grating spectrometers, also known as “double modulation technique” to the Fourier Transform Infrared (FTIR) machine. The essence of the technique is to add to the low-frequency time-delay modulation provided by the FTIR scanning mirror a further modulation of the pump beam intensity itself at a significantly higher frequency.

5. Experimental Set-up

The PL set-up at CTCH consists of an excitation arm, with a laser installed in a XYZ stage, a cryostat (Fig. 3), an optical collection arm, a Fourier Transform Infrared Spectroscopy machine (FTIR) for spectral analysis and an InSb detector. The excitation laser beam hits the heterostructure stimulating photoluminescence (PL) in the semiconductor. The temperature of the semiconductor can be turned into the cryostat with a PiD controlled resistor and a cold finger. The PL generated in the semiconductor is collected by a collimating lens and guided into a focusing lens which concentrates the signal at the defined focal point of the FTIR spectrometer input (Fig. 1, Fig. 2). An InSb detector collects the FTIR output. The detector signal can be traced in real time on an oscilloscope. This found its usage particularly during the alignment procedure. The lock-in amplifier differentiates the PL signal from the background. At the end the final PL spectrum is calculated based on the Fourier Transform by the commercial OPUS software.

5.1. Sample

IV-VI compounds are characterized by a narrow direct energy band-gap. This favors absorption and emission of photons on the edges of the band making them suitable for its application in mid-infrared optoelectronic devices. Besides, unusual test performed in bulk layers and other experimental structures, samples can be divided on active layer (AL) samples and short cavity (SC) samples. The former corresponds to a stack of PbSe QWs embedded in a PbSrSe matrix (Fig. 1). The later replicates the AL structures on top of a PbEuTe/EuTe Bragg mirror (Fig. 2). These structures imply that they should be measured in different set-up alignments.

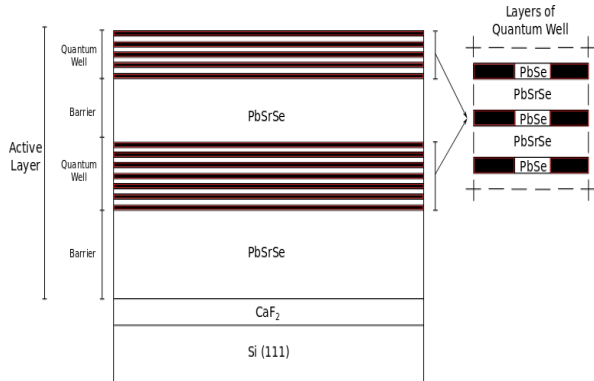


Fig. 5.1. Active layer sample

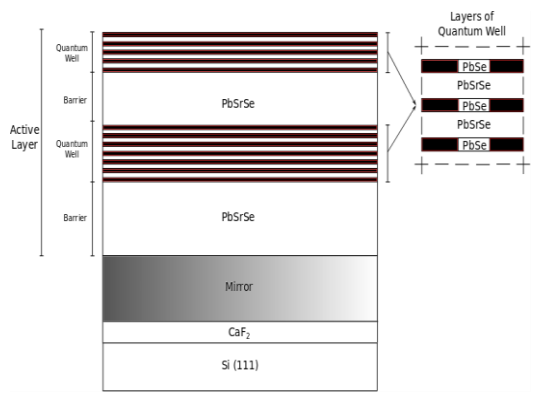


Fig. 5.2. Short cavity sample.

5.1.1. Sample Cleanliness and Mounting

Before mounting the sample in the sample holder, several steps were taken into account in order to both keep the cleanliness of the PL set-up and minimize the possible factors that affect the repeatability of the experiments.

Latex and nitrile gloves were always used while manipulating with the samples as well as clean assembly tweezers. Both sides of the sample were cleaned using acetone and isopropanol (propanol-2). To ensure that the sample holder is also clean, free of residuals like vacuum grease or photoresist, the sample holder was firstly cleaned with soap and hot water and then rinsed with previously mentioned solvents (acetone and isopropanol). Images of epitaxial layer were recorded with the Nomarsky microscope at the zoom magnitudes 5x, 20x and 40x to document any particular feature of interest.

Mounting was performed on a clean paper so even though sample would slip, it still was clean. A sample was put in the sample holder in a way the laser could hit the epitaxial side of the sample through a hole carved inside the sample holder and then a plate was put back on to fix the elements with screws. Thermo-conductivity grease on the bottom part of the sample holder was used to get a better heat conductivity during measurements. The sample holder was ready to be mounted in the cryostat with a direct contact with cold finger. The last step was to ensure that the cover is perfectly aligned with cryostat walls edges.

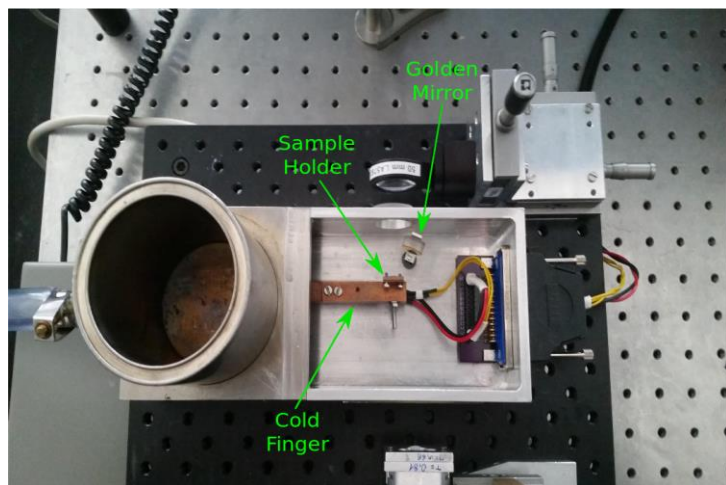


Fig. 5.3. Cryostat.

5.2. Alignment

There are two available set-up alignments to measure PL at the CTCH spectroscopy lab. One exciting the semiconductor through its substrate and the other, after reflection in an Au mirror, through the semiconductor epilayer top surface. Even though the first one is easier to align, it is not compatible with samples composed of an AL grown on top of a PbEuTe/EuTe mirror (SC). This is because of the low transmission of the IV-VI Bragg mirror at the laser excitation wavelength ($1.55 \mu\text{m}$).

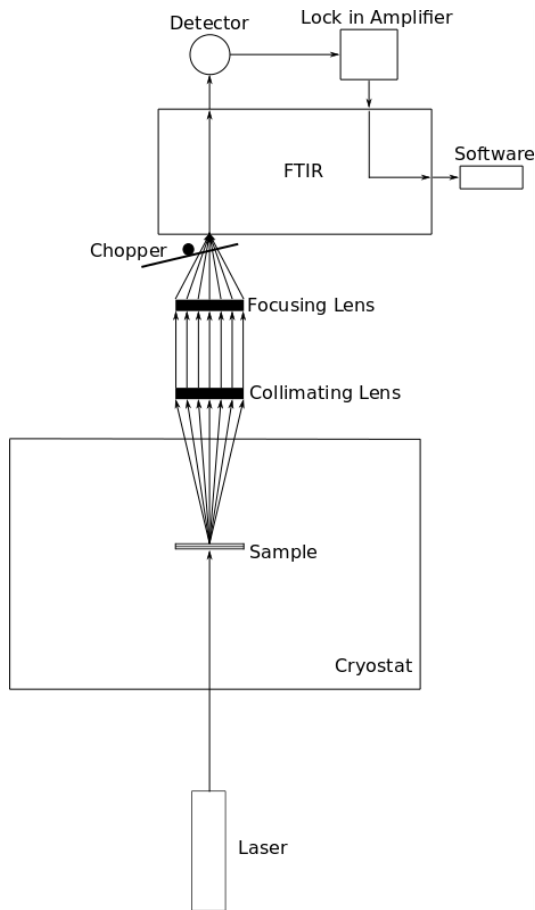


Fig. 5.4. Set-up for AL.

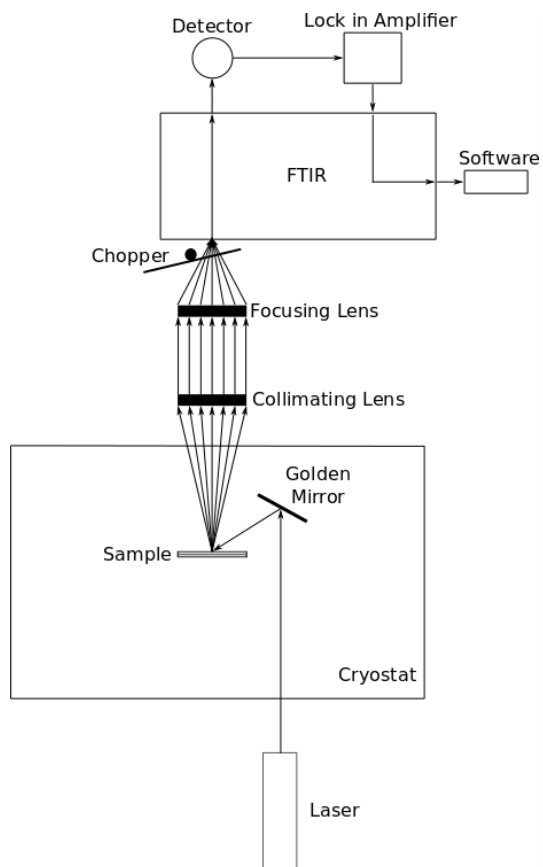


Fig. 5.5. Set-up for AL and SC.

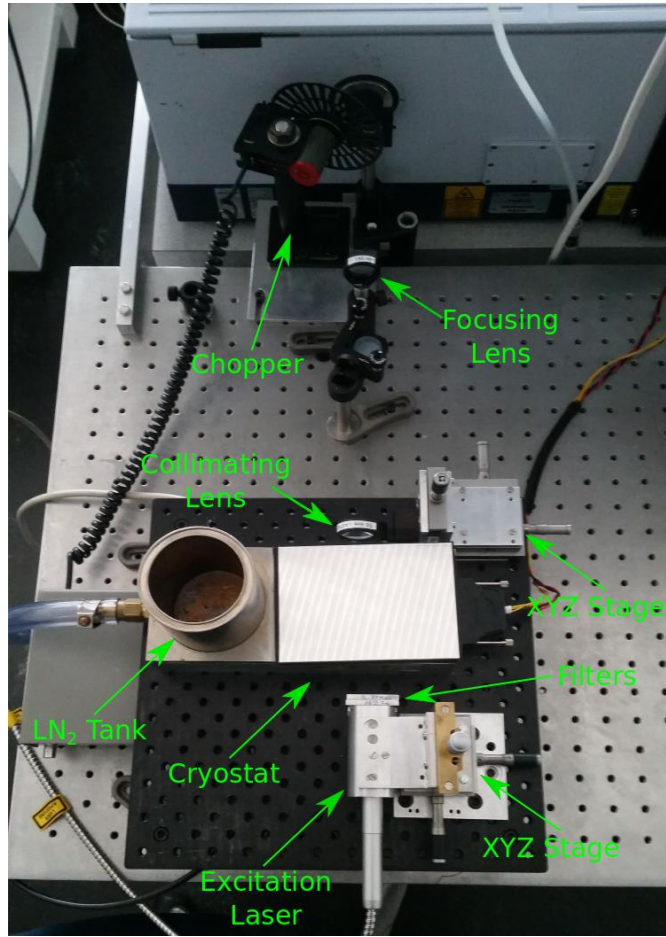


Fig. 5.5. Set-up for AL and SC.

Aligning procedure involved using IRIS, an object which allows easy beam positioning. To achieve the most optimal PL signal, IRIS was moved from collimating lens up to the FTiR so that the laser beam still passed through the tiny hole. The alignment of PL set-up required establishing the focal distance (125mm) + 2mm between the cryostat output and FTiR input. Three movable stages were also used for aligning manipulation. Because the pumping laser was really powerful, filters 0.81 and 0.69 were used in order to avoid damaging samples. Lastly, the chopper was placed at a little angle (around 20°-30°) to avoid reflections.

5.3. FTIR (Fourier Transform Infrared) Spectrometer

FTIR is the abbreviation of Fourier Transform Infra-Red, a method of infrared spectroscopy to obtain infrared spectrum of absorption and emission of a given sample – either solid, liquid or gas. The mathematical Fourier Transform algorithm is used to convert the raw data into the spectrum. In comparison to older technology, the FTIR measures all of the infrared frequencies simultaneously which results in scanning time decrease. This is achieved by an interferometer which produces a unique type of signal which is already encoded in all infrared frequencies.

FTIR provides the information needed to identify the unknown sample as well as determination of the quality or consistency and amount of components in the specified sample.

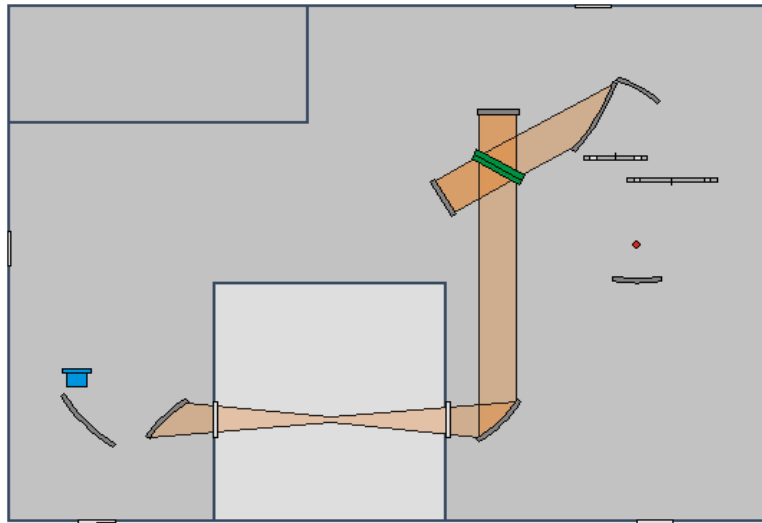


Fig. 5.6. Beam path inside the FTIR.

5.4. Nomarsky Microscope

To record images of epitaxial layer, the Nomarsky microscope was used. Nomarsky microscopy was invented by Polish physicist Georges (Jerzy) Nomarski specialized in theoretical optics in mid-1950s. Nomarski Microscopy also called NIC (Nomarski Interface Contrast) or DIC (Differential Interface Contrast) is an optical microscopy technique of deriving and enhancing contrast in unstained, transparent, samples from differences in index of reflection of specimen components. Improved contrast in the image can be achieved because differential interface contrast transforms optical path gradients of specimen into amplitude differences.

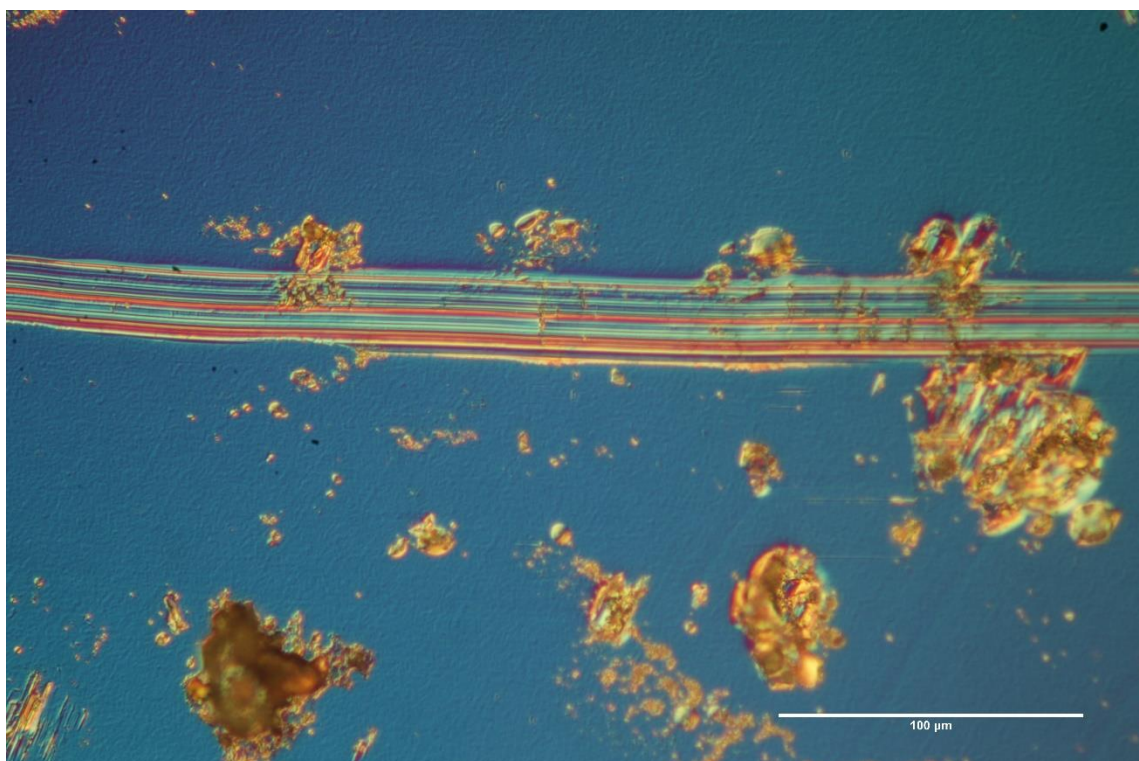


Fig. 5.7. Exemplary image taken by Nomarsky microscope.

5.5. Pumps

PL characterization at cryogenic temperatures requires low pressure conditions. The home-designed pumping system of the PL set-up at CTCH consists of a pre-vacuum pump (rotary) and pfeiffer turbo pump (model TMU 065). The system pressure could be controlled during the operation with a full range manometer (model TPG 261). Vacuum systems are relatively delicate and their manipulation entails certain risks for the set-up.



Fig. 5.8. Turbo pump electronics control.

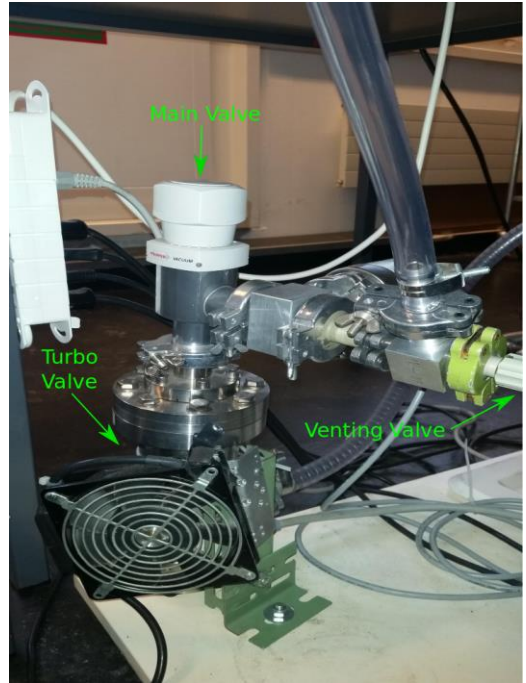


Fig. 5.9. Pumps and valves.

5.6. Lock-In Amplifier and Chopper

Lock-in amplifier is used to measure and detect very small alternating current signals to few nanovolts. It is possible to get accurate measurements even if the signal is much smaller than noise sources. The technique which is used in lock-in amplifier is called phase-sensitive detection. It marks out the component of the signal at a specific reference phase and frequency. If the reference frequency is different than frequency of noise signals, then they do not affect the measurement because they are rejected. Lock-in amplifier is an extended tool to measure extremely small signals in the presence of an overwhelming background. It is possible to get accurate measurements even if the signal is much smaller than the noise sources. The technique which is used in lock-in amplifier is called phase-sensitive detection. It defines the component of the signal at a specific reference phase and frequency.

To achieve a working connection, the detector collecting the signal was connected to lock-in amplifier and extended to the oscilloscope input socket using BNC cables. To differentiate the signal from the background, the reference frequency was needed to be delivered to the lock-in amplifier. Chopper controller was connected to lock-in amplifier and extended to the oscilloscope input socket. And so, the oscilloscope was able to indicate the output signal and frequency. What is more, voltmeter was connected to lock-in amplifier.

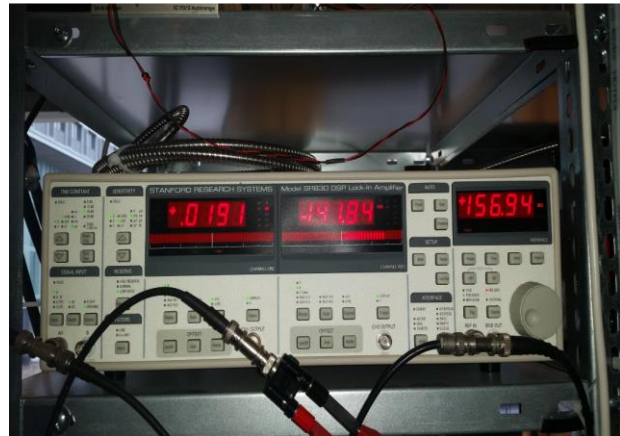


Fig. 5.10. Lock-in amplifier.

The optical chopper SR540 from Stanford Research Systems is used to modulate the intensity of optical signals which can be chopped at rates varying from 4 Hz to 4000 Hz. The Chopper frequency must be kept well above the one of the FTIR mirror.



Fig. 5.11 Chopper.

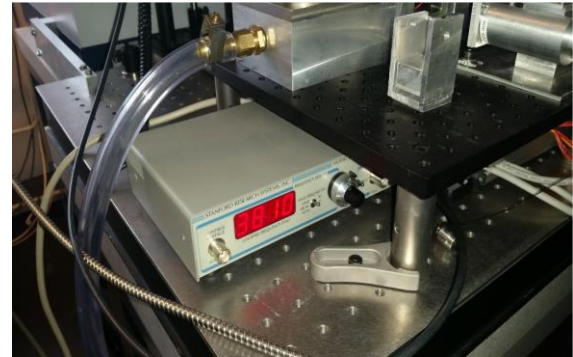


Fig. 5.12. Chopper controller.

5.7. Oscilloscope

Oscilloscope allows monitoring signals as a function of time displayed on a two-dimensional graph, making it a useful tool during the set-up adjustment and alignment because the PL changes can be observed directly on the screen in real time.

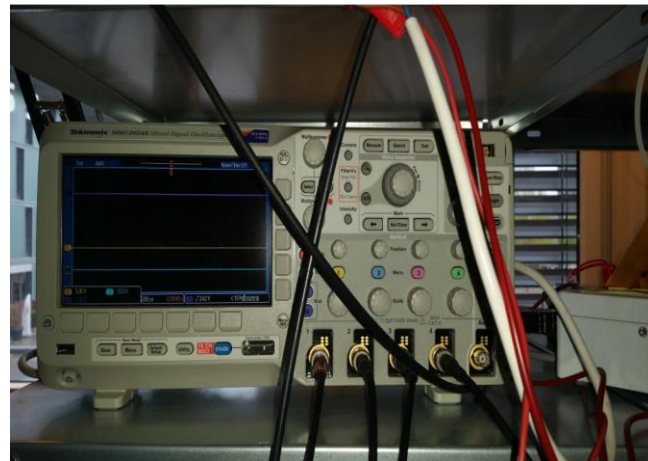


Fig. 5.13. Oscilloscope.

5.8. Detector

The detector which was used in this set-up was InSb photodiode/amplifier designed for low frequency DC or chopped measurements. The model number is IS-020-E-LN6N from Electro-Optical Systems Inc. The detector operates at $1.0\mu\text{m}$ to $5.5\mu\text{m}$ spectral range with the 2mm diameter of active area. Before turning the detector on, it was important to fill the metal dewar with liquid nitrogen by the fill funnel.

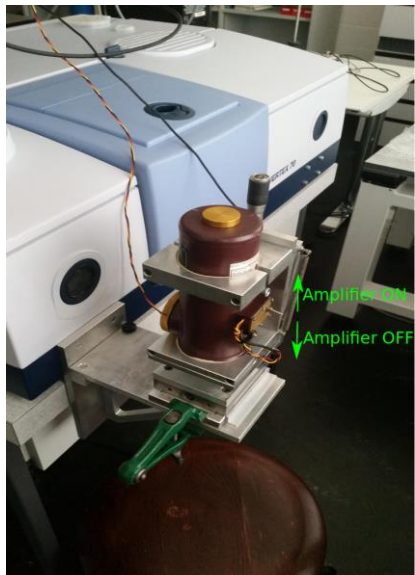


Fig. 5.14. Detector.

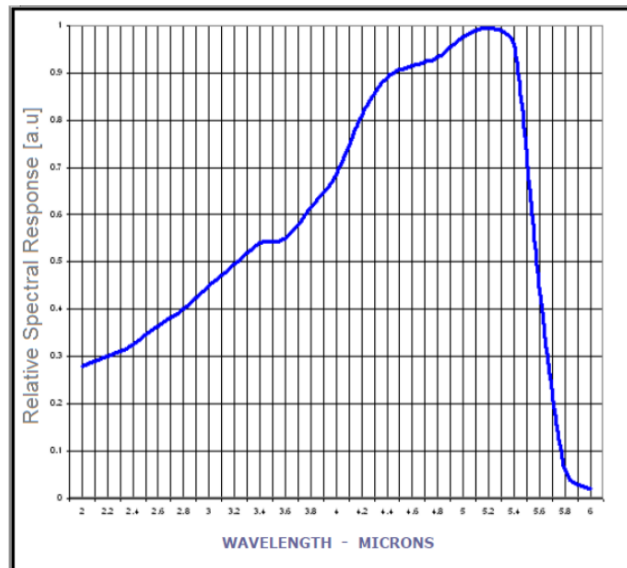


Fig. 5.15. InSb relative spectral response.

5.9. Temperature Controls

Operating temperature ranged between 100K and 300K. To cool down the sample, liquid nitrogen was purred into the LN_2 tank.



Fig. 5.16. Temperature controls.

5.10. Laser

The laser operates at $1.55\mu\text{m}$ and starts lasing at around 1.5V. In order to avoid burning a sample, it was taken into consideration not to exceed higher excitation powers than 4.5V for filters 0.69 and 0.81. The laser has been modified in the way to be operated both in pulse mode or continuous-wave mode.

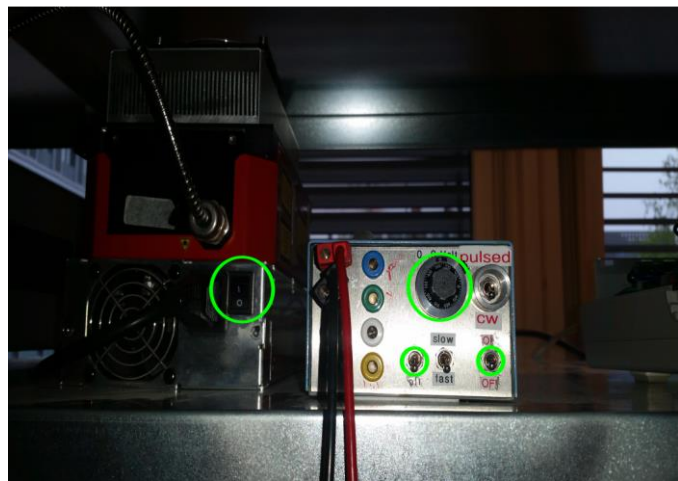


Fig. 5.17. Laser supply.

III. Research Part

6. Photoluminescence of PbSe/PbSrSe Semiconductor Materials in IR

The research section has been divided into three sub-parts. The first part concerns the reliability determination of the set-up which was used to conduct PL measurements. In the second part, efforts were made to investigate what are the effects of applying different number of QWs and so in the third part, what are the effects of applying different content of strontium (Sr).

6.1. Set-up Reliability Check

The aim of this experiment, was to determine the reproducibility and the reliability of the PL set-up. The PL of active layer sample was measured three times in the same experimental conditions. The results of each measurement were then compared. The PL of the sample was excited by the pumping laser operating at $\lambda=1.55\mu\text{m}$ at three different power excitations - 2.50V, 3.50V and 4.50V. The pressure was maintained between 10E-4 bars and 10E-3bars. The modulation frequency of the excitation laser was set to 3800Hz. This value was chosen because the chopper frequency had to be few times higher than Fourier frequency of the FTIR scanning mirror. The measurement was performed on the temperature range from 125K and 300K with a 25K step. Each time the measurement was finished, the sample was taken out and mounted again.

Experimental Conditions	
Pressure	10E-4 - 10E-3
Pump Laser	1.55 μm
Chopper Frequency	3800Hz
LIA Sensitivity	20mV, 50mV
Power Excitation	2.50V, 3.50V, 4.50V
Temperature	125K, 150K, 175K, 200K, 225K, 250K, 275K, 300K

Sample used for this measurement was labelled as 1708 and was an AL sample with MQWs system semiconductor material grown on silicon substrate at Sr content equal to 6.05%. The number of quantum wells was equal to 7+5 with thickness of 5.5nm whereas the number of barriers was equal to 6+4 with thickness of 15nm.

Sample Description	
Sample No.	1708
Substrate	Si(111)
Material	PbSe/PbSrSe
Strontium Content	6.05 %
Number of QWs	7+5
QW Thickness	5.5 nm
Barriers	6+4
Barrier Thickness	15nm

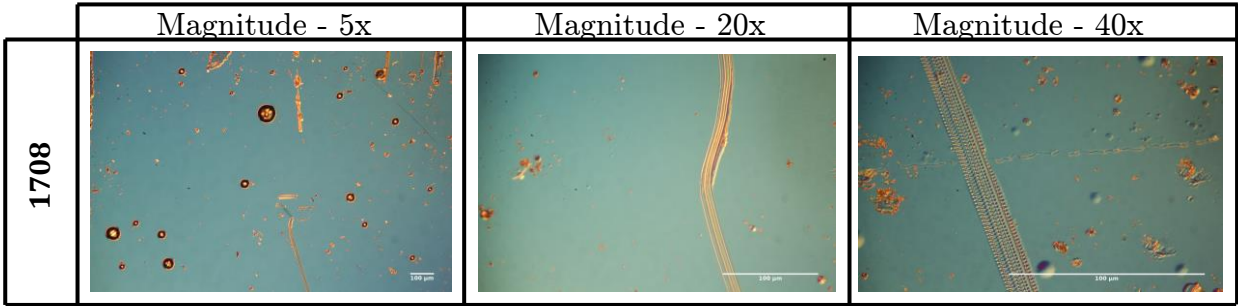


Fig. 6.1. Images of the epitaxial layer.

Above images show the surface after the third measurement. Radius of circular irregularities ranges from $20\mu m$ up to $50\mu m$. The width of longitudinal irregularities equals approximately $10\mu m$. Of course, those scratches are caused by a human factor, namely mounting and dismounting which was performed multiple times and impacts the discrepancies between each measurement.

The figures presented below (fig. 6.2, 6.3, 6.4) show the PL spectra and are the combination of three independent measurements at a specific power excitation.

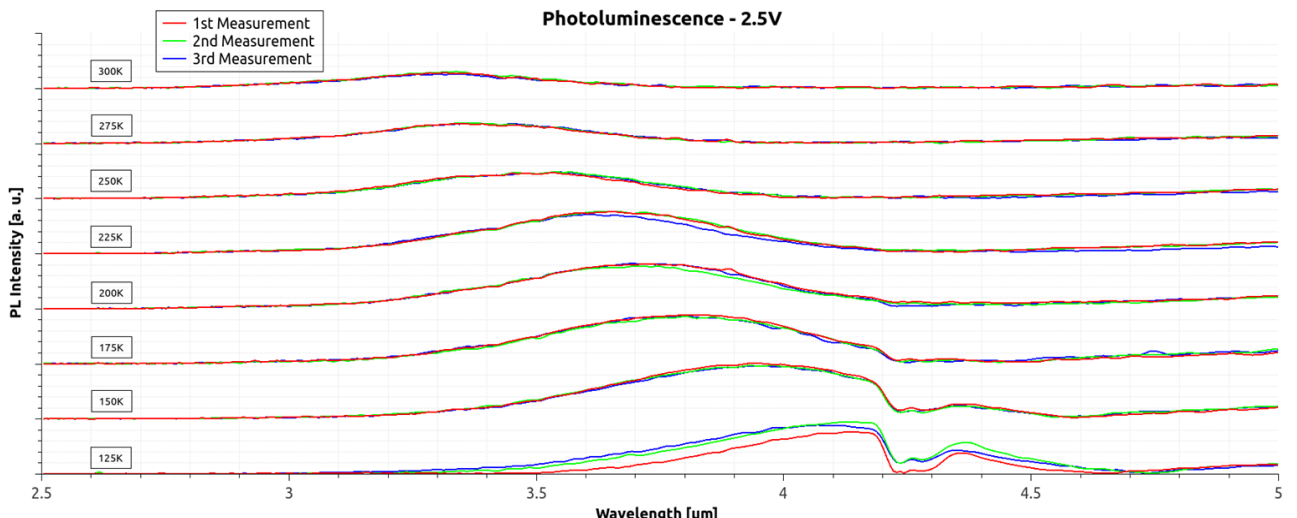


Fig. 6.2. PL spectra at 2.50V.

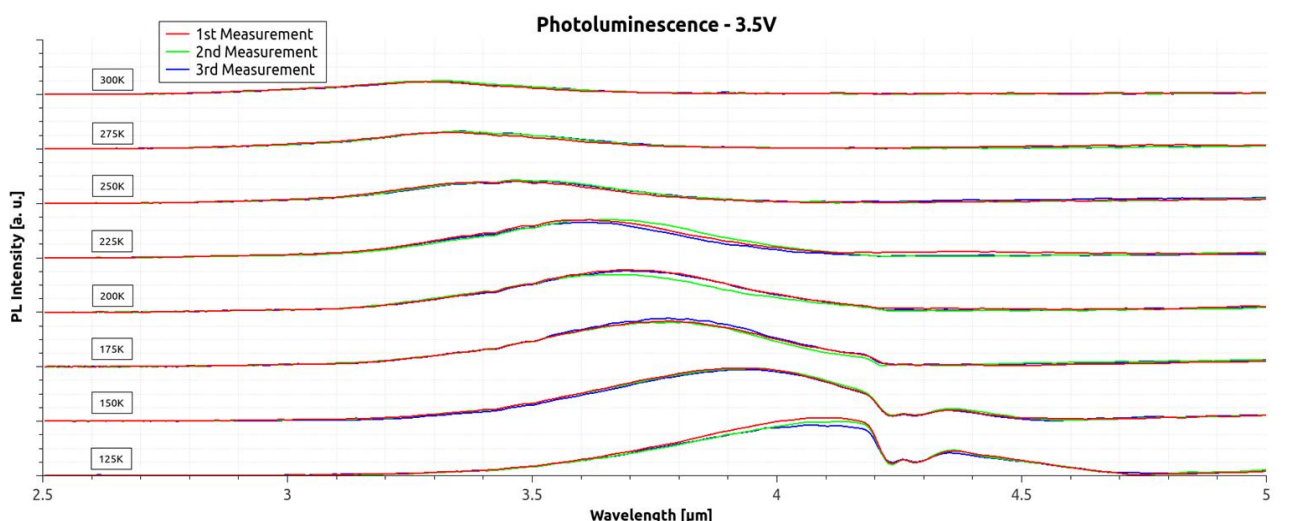


Fig. 6.3. PL spectra at 3.50V.

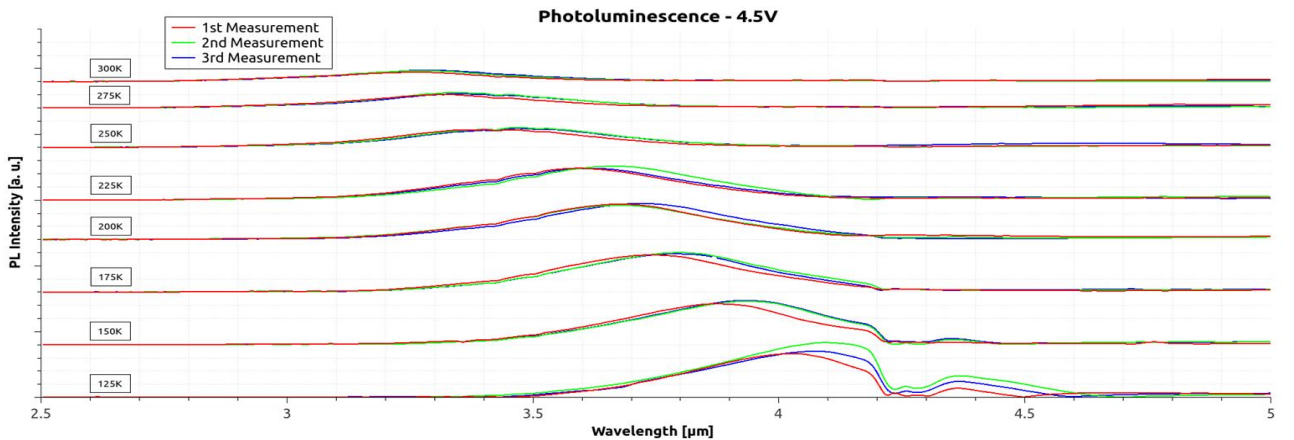


Fig. 6.4. PL spectra at 4.50V.

As it can be seen, for high temperatures the results were nearly the same. Variations of PL intensity start appearing at 300K for 2.50V and 3.50V. For 4.50V the variations are much more noticeable. To quantify the exact change, the integrated intensity depending on temperature was determined for specific power excitations (fig. 6.5, 6.6, 6.7).

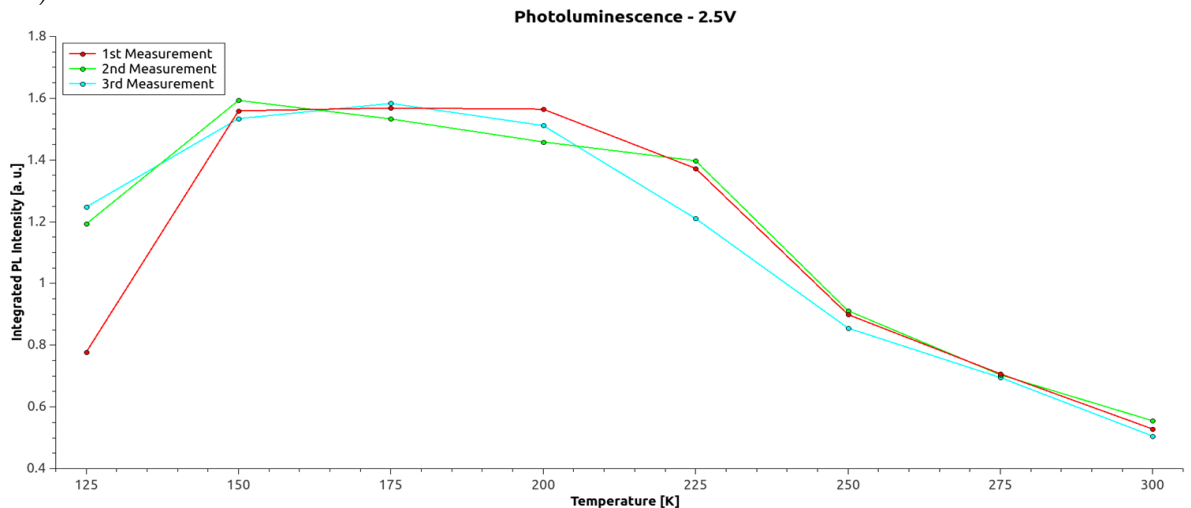


Fig. 6.5. PL intensities at 2.50V.

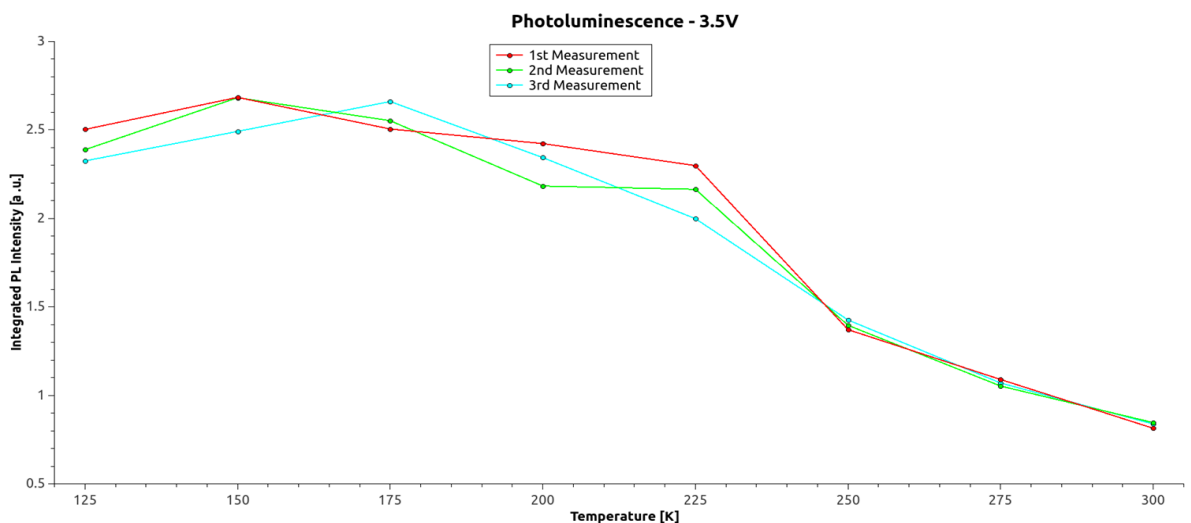


Fig. 6.6. PL intensities at 3.50V.

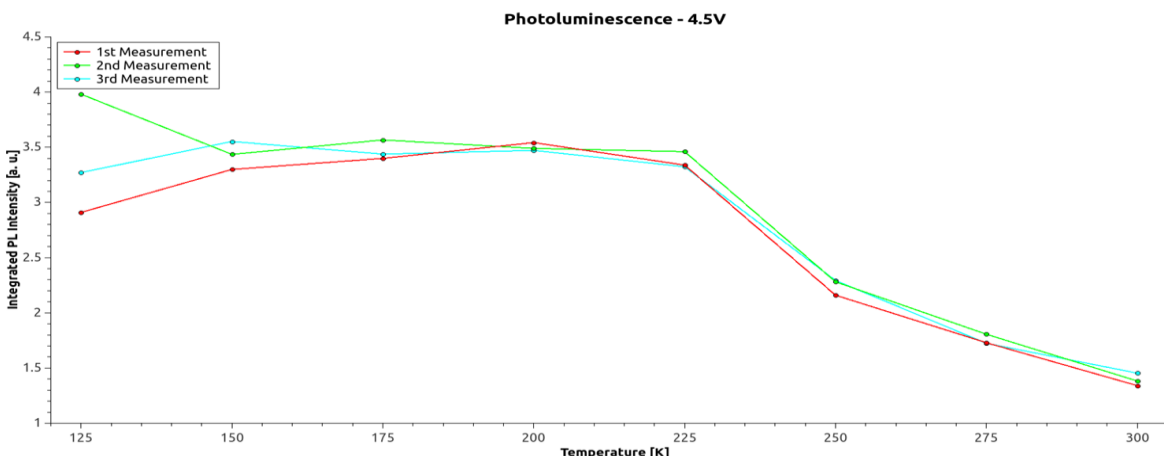


Fig. 6.7. PL intensities at 4.50V.

As expected, the highest intensity was achieved at lower temperatures. Looking at the graphs, it may be noticed that at the temperature of 225K, there is a steep drop. This drop is caused by critical temperature. It is a temperature where electrons possess enough kinetic energy to be able to leave the quantum well resulting in a lower rate of recombinations causing lower PL emission.

The same procedure was performed to determine the peak energy depending on the temperature (figures 6.8, 6.9, 6.10).

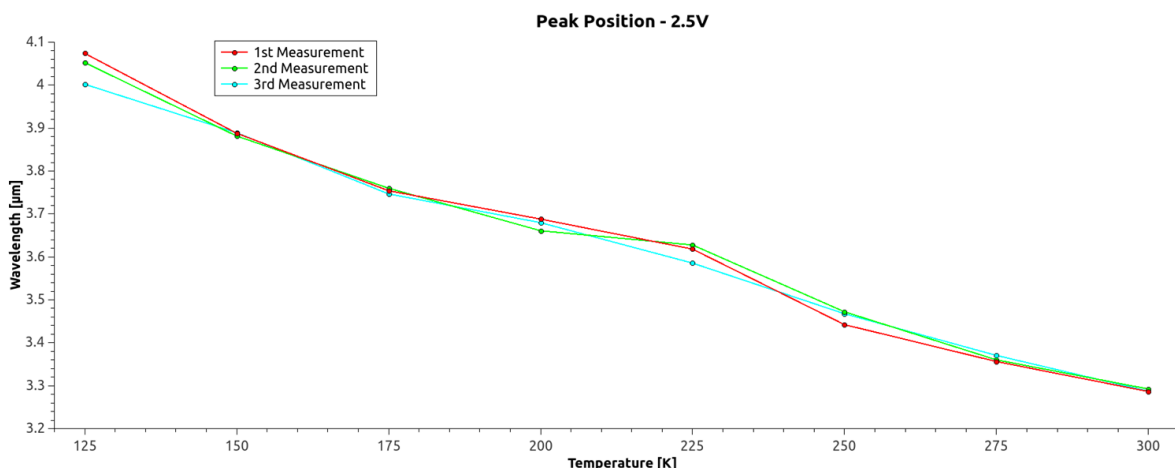


Fig. 6.8. Energies at 2.50V.

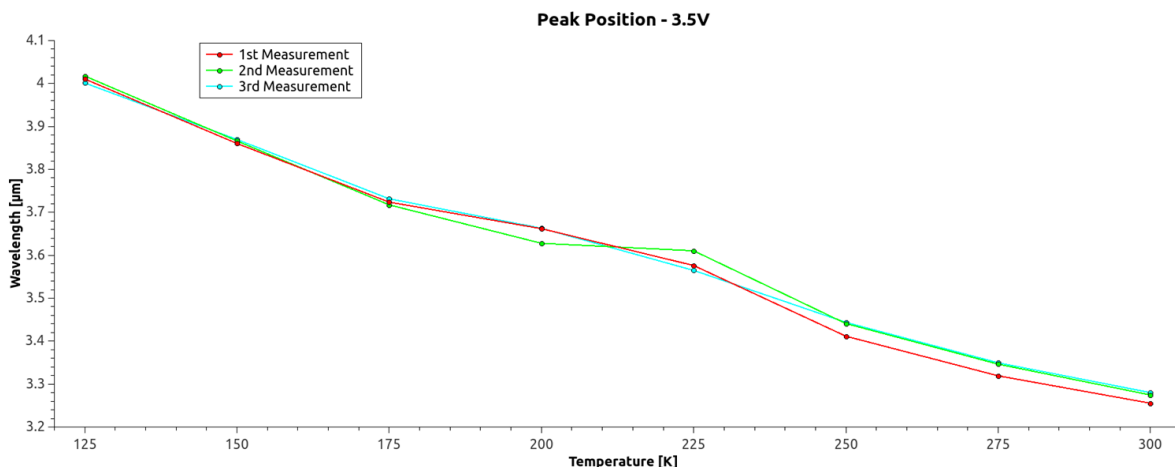


Fig. 6.9. Energies at 3.50V.

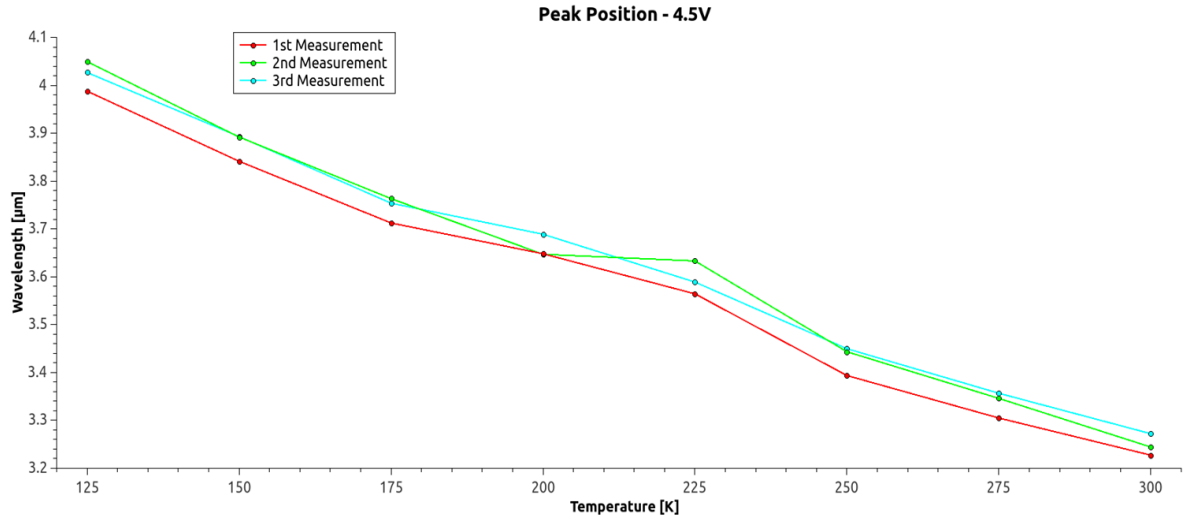


Fig. 6.10. Energies at 4.50V.

To quantify the error, standard deviation as well as standard error have been calculated for a specific power excitations and temperatures.

Power Excitation – 2.5V								
Temperature [K]	125	150	175	200	225	250	275	300
1 st Peak	4.074	3.888	3.754	3.688	3.618	3.442	3.356	3.286
2 nd Peak	4.053	3.882	3.760	3.661	3.628	3.472	3.360	3.292
3 rd Peak	4.002	3.889	3.747	3.680	3.586	3.468	3.371	3.287
Average Peak	4.043	3.886	3.754	3.676	3.610	3.461	3.362	3.289
St. Dev. Peak	0.037	0.004	0.007	0.014	0.022	0.016	0.007	0.003
St. Error Peak	0.021	0.002	0.004	0.008	0.013	0.009	0.004	0.002
1 st Intensity	0.777	1.559	1.569	1.564	1.373	0.899	0.707	0.528
2 nd Intensity	1.193	1.593	1.533	1.458	1.398	0.912	0.704	0.555
3 rd Intensity	1.247	1.534	1.583	1.511	1.210	0.855	0.695	0.505
Average Intensity	1.072	1.562	1.562	1.511	1.327	0.889	0.702	0.530
St. Dev. Intensity	0.257	0.030	0.026	0.053	0.102	0.030	0.006	0.025
St. Error Intensity	0.148	0.017	0.015	0.031	0.059	0.017	0.004	0.014

Power Excitation – 3.5V								
Temperature [K]	125	150	175	200	225	250	275	300
1 st Peak	4.010	3.860	3.724	3.662	3.576	3.411	3.319	3.255
2 nd Peak	4.017	3.866	3.717	3.628	3.610	3.441	3.346	3.275
3 rd Peak	4.001	3.870	3.732	3.663	3.565	3.444	3.350	3.280
Average Peak	4.010	3.865	3.724	3.651	3.584	3.432	3.338	3.270
St. Dev. Peak	0.008	0.005	0.007	0.020	0.024	0.018	0.017	0.013
St. Error Peak	0.005	0.003	0.004	0.012	0.014	0.010	0.010	0.007
1 st Intensity	2.503	2.684	2.505	2.423	2.299	1.372	1.090	0.814
2 nd Intensity	2.388	2.682	2.552	2.183	2.165	1.396	1.053	0.846
3 rd Intensity	2.325	2.492	2.661	2.344	1.999	1.426	1.070	0.838
Average Intensity	2.406	2.620	2.573	2.317	2.154	1.398	1.071	0.833
St. Dev. Intensity	0.090	0.111	0.080	0.122	0.150	0.027	0.019	0.017
St. Error Intensity	0.052	0.064	0.046	0.071	0.087	0.016	0.011	0.010

Power Excitation – 4.5V								
Temperature [K]	125	150	175	200	225	250	275	300
1 st Peak	3.988	3.841	3.712	3.648	3.564	3.394	3.305	3.227
2 nd Peak	4.050	3.892	3.763	3.647	3.633	3.443	3.346	3.244
3 rd Peak	4.027	3.893	3.754	3.689	3.589	3.450	3.357	3.272
Average Peak	4.021	3.875	3.743	3.661	3.595	3.429	3.336	3.248
St. Dev. Peak	0.031	0.030	0.027	0.024	0.035	0.031	0.027	0.023
St. Error Peak	0.018	0.017	0.016	0.014	0.020	0.018	0.016	0.013
1 st Intensity	2.910	3.299	3.399	3.543	3.339	2.160	1.729	1.340
2 nd Intensity	3.981	3.436	3.567	3.490	3.461	2.281	1.806	1.382
3 rd Intensity	3.271	3.553	3.438	3.472	3.324	2.293	1.723	1.453
Average Intensity	3.387	3.429	3.468	3.502	3.374	2.245	1.753	1.392
St. Dev. Intensity	0.545	0.127	0.088	0.037	0.075	0.074	0.046	0.057
St. Error Intensity	0.315	0.073	0.051	0.021	0.043	0.043	0.027	0.033

Fig. 6.11. Results.

The PL set-up reproducibility in terms of intensity is equal to 95.32% whereas in case of PL energy it is equal to 99.48%. It might be concluded that the set-up is very accurate, reliable and repeatable. The small deviation may be caused by additional scratches over a surface while dismounting and mounting again as well as by human factors.

Recently, the PL set-up has been improved, namely the pumping system and the temperature system have been improved while InSb detector has been changed. The PL system might be even more reliable now.

6.2. Number of Quantum Wells

The goal of this experiment was to study dependences of quantum wells number and to investigate the uniformity of semiconductor QW stacks grown by MBE method. Four active layer samples with different quantum well numbers were measured.

The experimental set-up settings have not been changed. The only difference was an addition of 100mV lock-in amplifier sensitivity because of high PL emission.

Experimental Conditions	
Pressure	10E-4 - 10E-3
Pump Laser	1.55μm
Chopper Frequency	3800Hz
LIA Sensitivity	20mV, 50mV, 100mV
Power Excitation	2.50V, 3.50V, 4.50V
Temperature	125K, 150K, 175K, 200K, 225K, 250K, 275K, 300K

Samples provided for this experiment were designated as 1716, 1717, 1718 and 1788 with number of quantum wells equal to 1, 3, 5 and 10 and Sr content equal to 6.70%, 6.60%, 6.30% and 8.30% respectively. The thickness of quantum well was 5.5nm whereas the thickness of barriers was 15nm for all the samples.

Sample Description				
Sample No.	1716	1717	1718	1788
Substrate	Si(111)	Si(111)	Si(111)	Si(111)
Material	PbSe/PbSrSe	PbSe/PbSrSe	PbSe/PbSrSe	PbSe/PbSrSe
Strontium Content	6.70 %	6.60 %	6.30 %	8.30 %
Number of QWs	1	3	5	10
QW Thickness	5.5 nm	5.5 nm	5.5 nm	5.5 nm
Barriers	-	2	4	9
Barrier Thickness	-	15nm	15nm	15nm

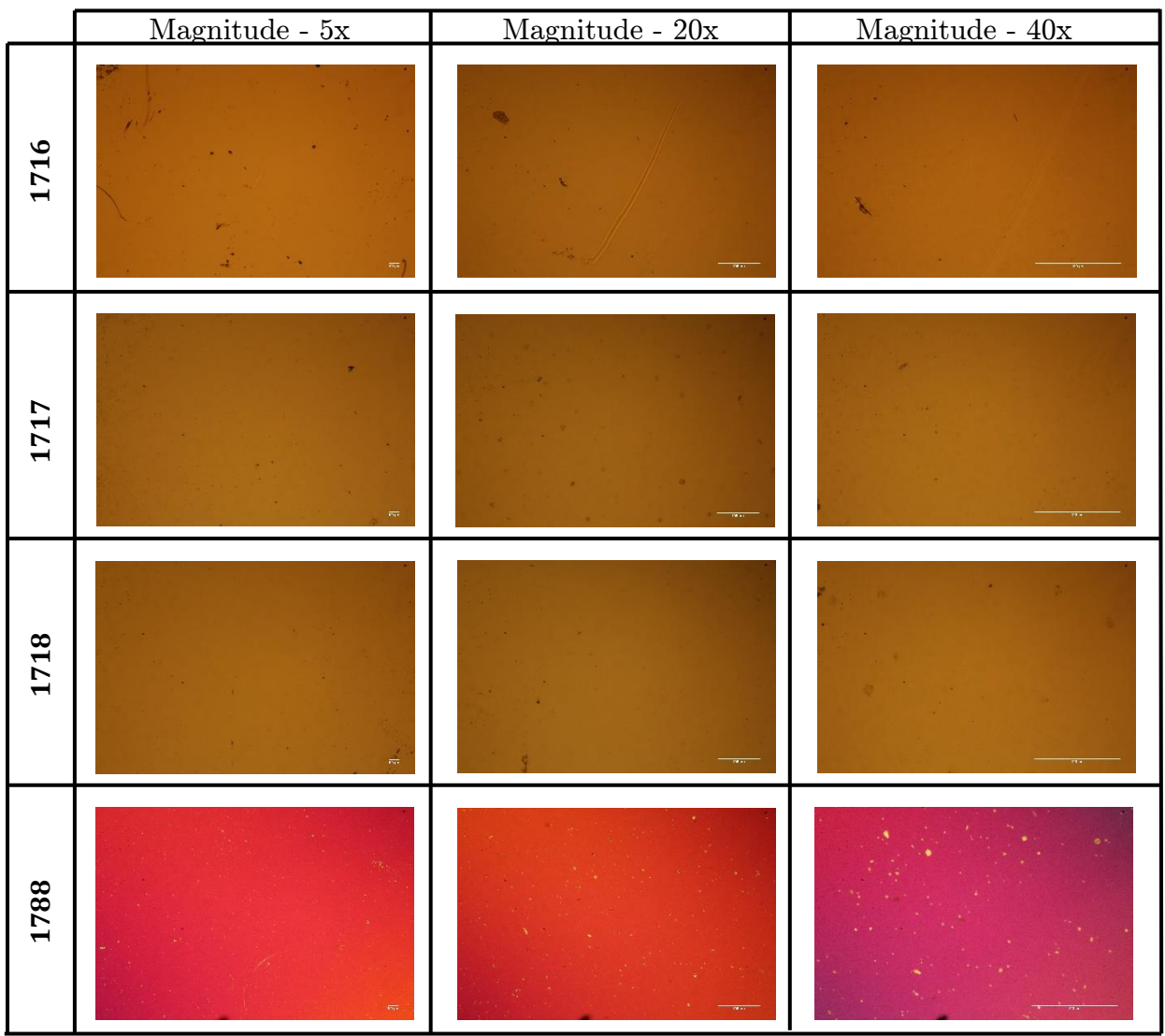


Fig. 6.12. Images of the epitaxial layers.

Above set of images (fig. 6.12) shows well-preserved surfaces of investigated samples. Radius of circular irregularities and width of longitudinal irregularities do not exceed $5 \mu\text{m}$. It may be noted, that in comparison to the previous measurement of sample 1708 where the scratches were 10 times bigger and had a significant impact, here the irregularities have negligible effect on conducted PL measurements.

Figures 6.13, 6.14 and 6.15 represent the results of the integrated PL intensity depending on the temperature.

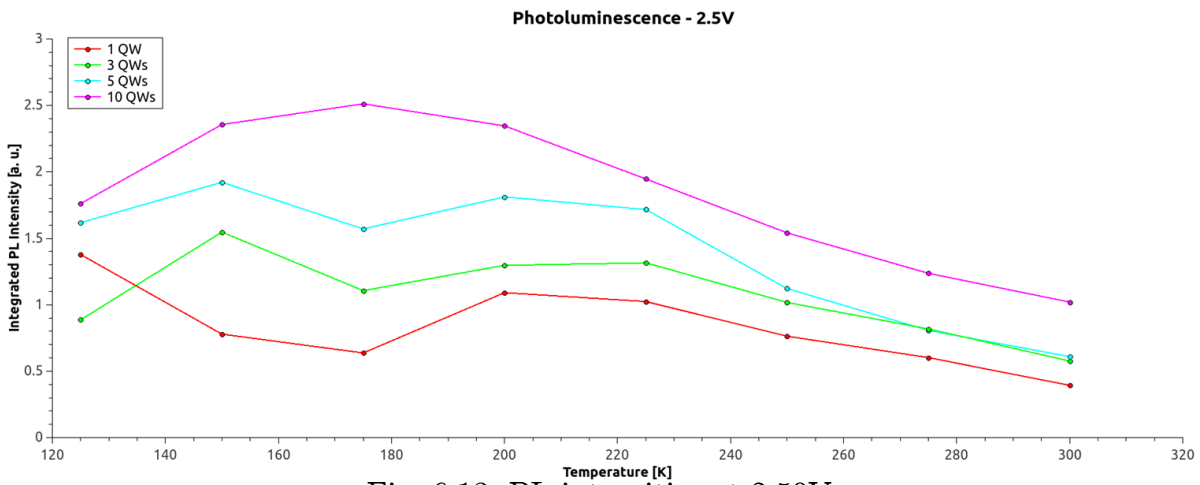


Fig. 6.13. PL intensities at 2.50V.

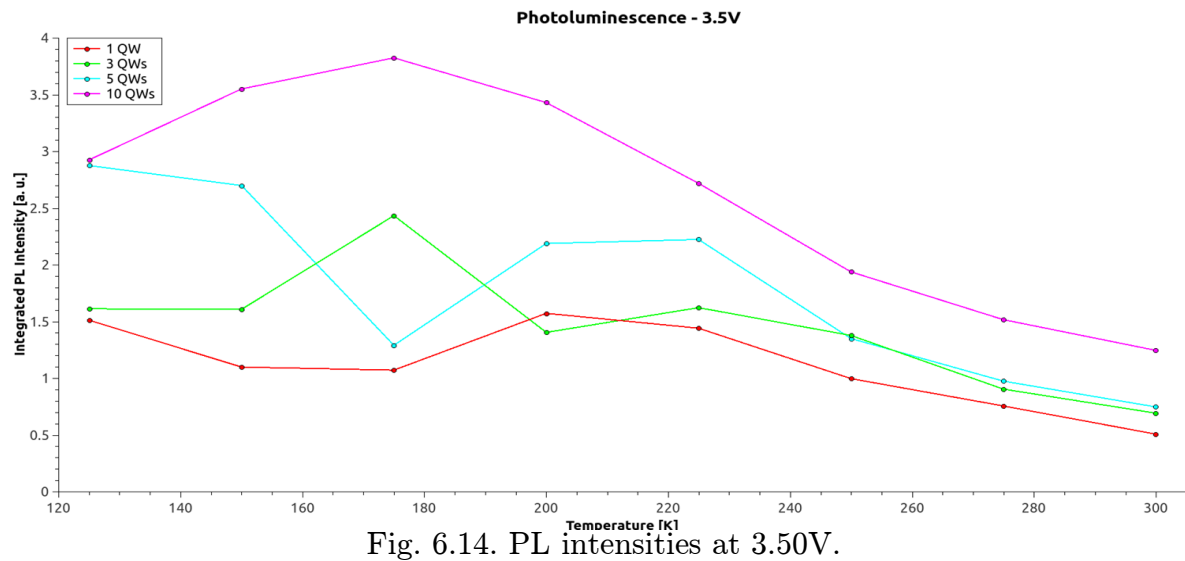


Fig. 6.14. PL intensities at 3.50V.

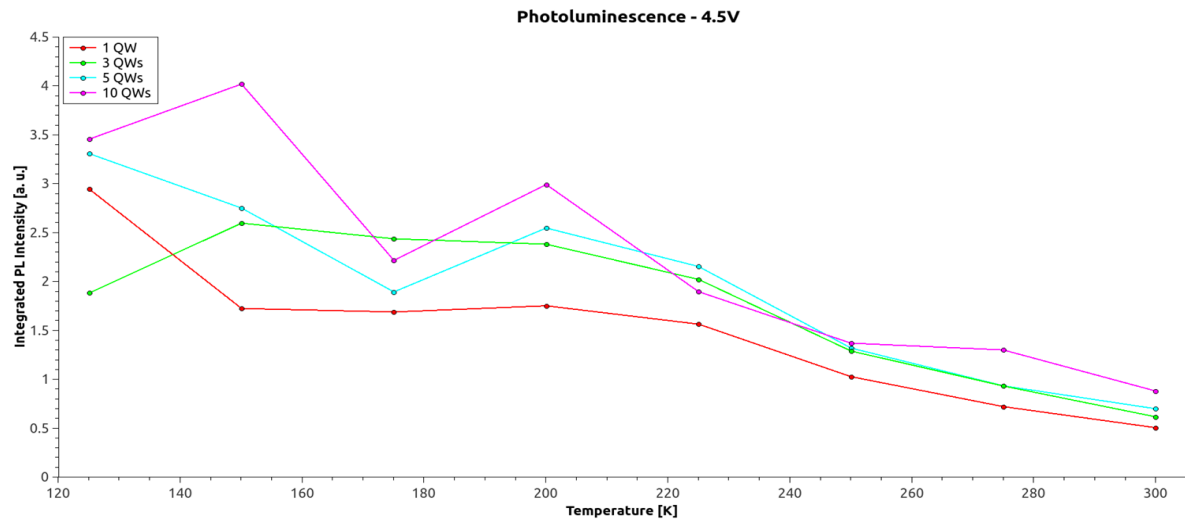


Fig. 6.15 PL intensities at 4.50V.

Presented graphs clearly show that the higher the number of quantum wells, the higher the PL intensity. This proves that high amount of quantum wells favors higher number of recombinations. To determine the uniformity of multiple number of QWs, the full width at half maximum (FWHM) was checked (fig. 6.16, 6.17 and 6.18).

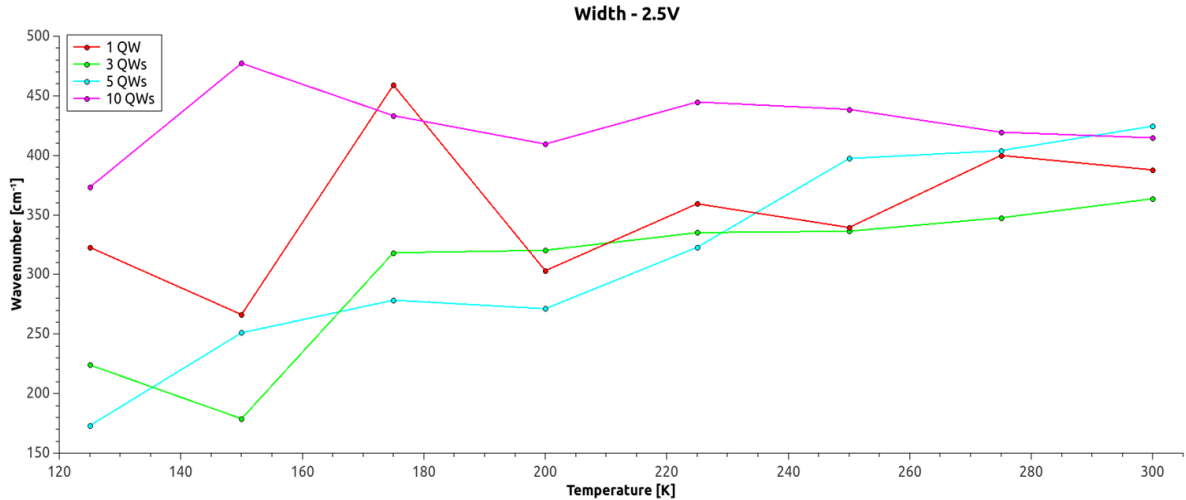


Fig. 6.16. FWHM at 2.50V.

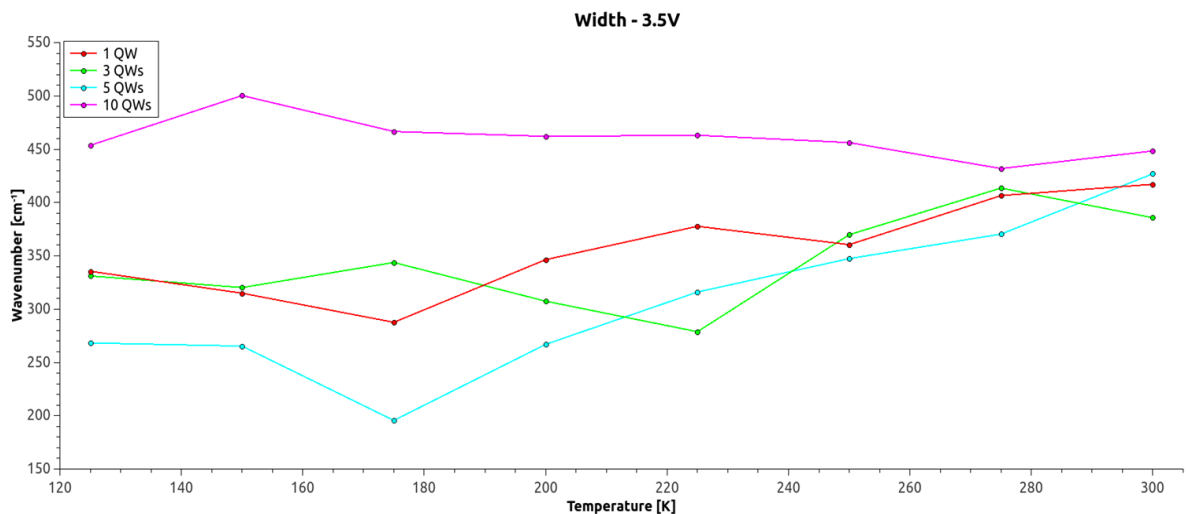


Fig. 6.17. FWHM at 3.50V.

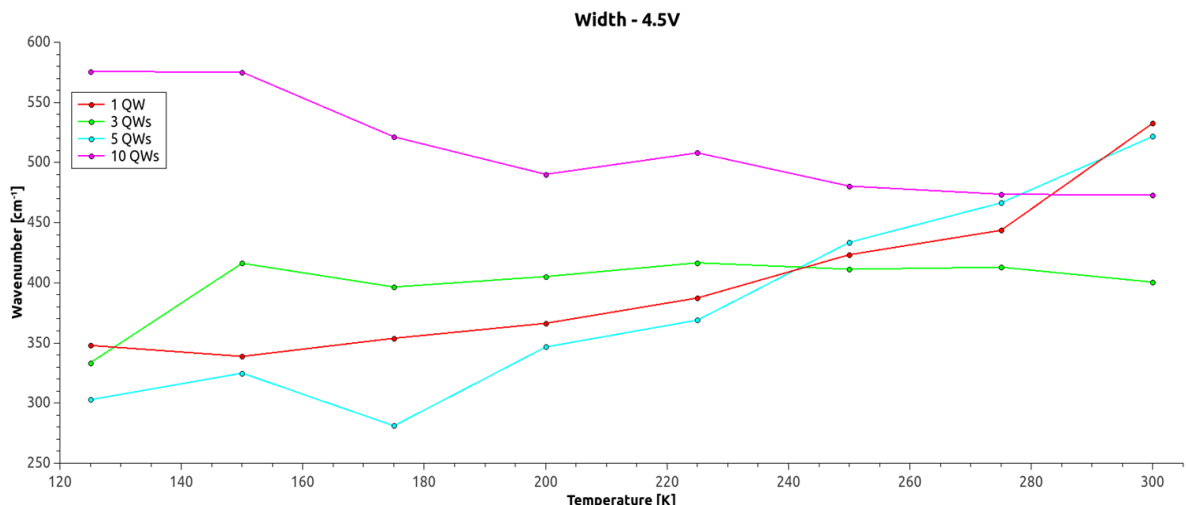


Fig. 6.18. FWHM at 4.50V.

For samples with 1, 3 and 5 QWs the width is comparable while for 10 QWs sample we may see that the difference is significant – the width is the highest for almost all temperatures. This is caused by overlapping of PL spectra for each quantum well. At low temperatures, the difference is the most noticeable but with the evolution of temperature towards higher temperatures, the width behavior tends to get similar for all the samples. This leads to a conclusion that high amount of quantum wells is not efficient for a room temperature.

Then, the peak energy was determined for each power excitation (fig. 6.19, 6.20 and 6.21).

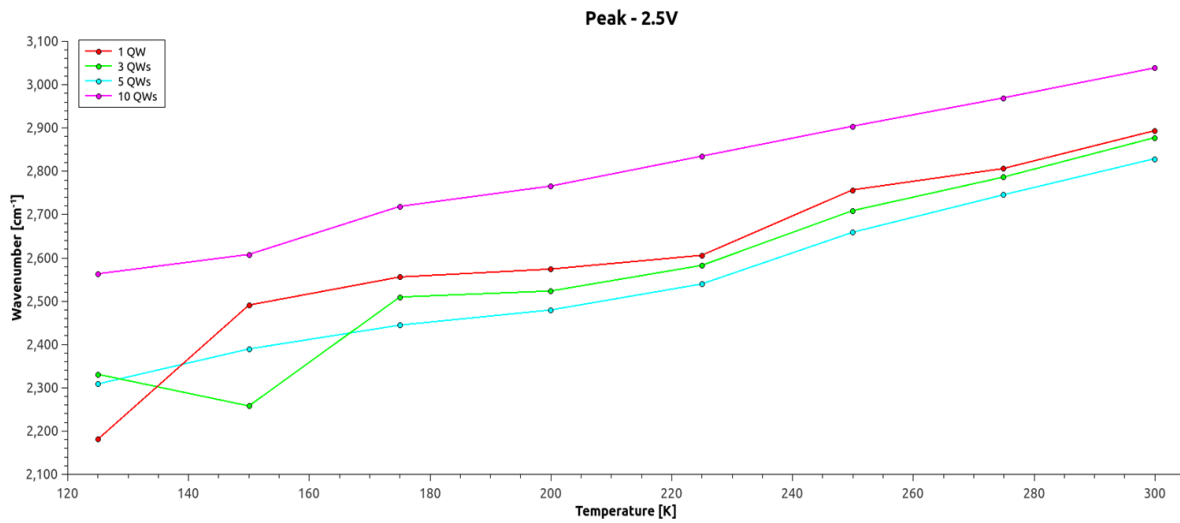


Fig. 6.19. Energies at 2.50V.

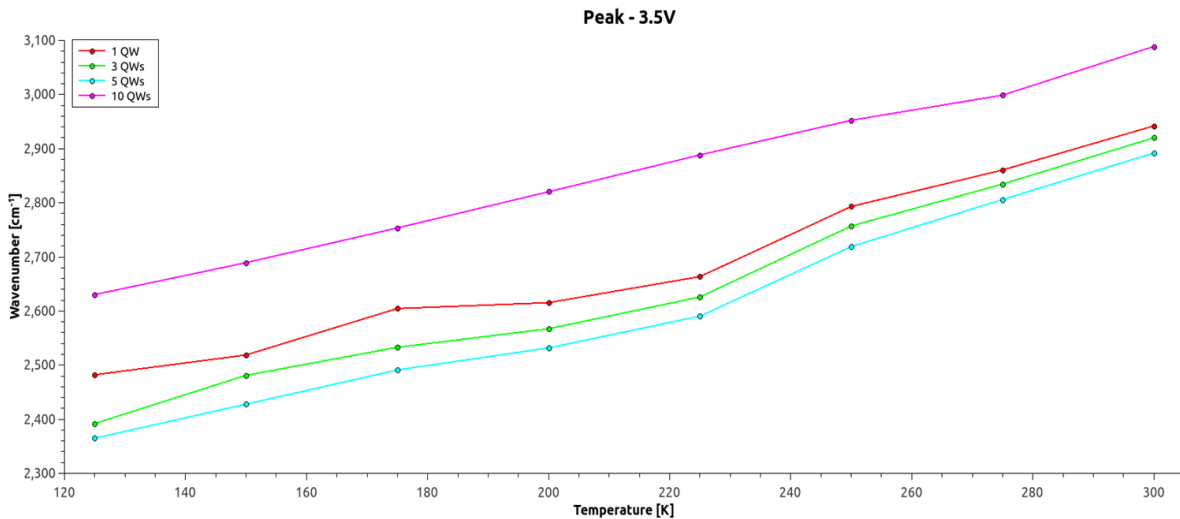


Fig. 6.20. Energies at 3.50V.

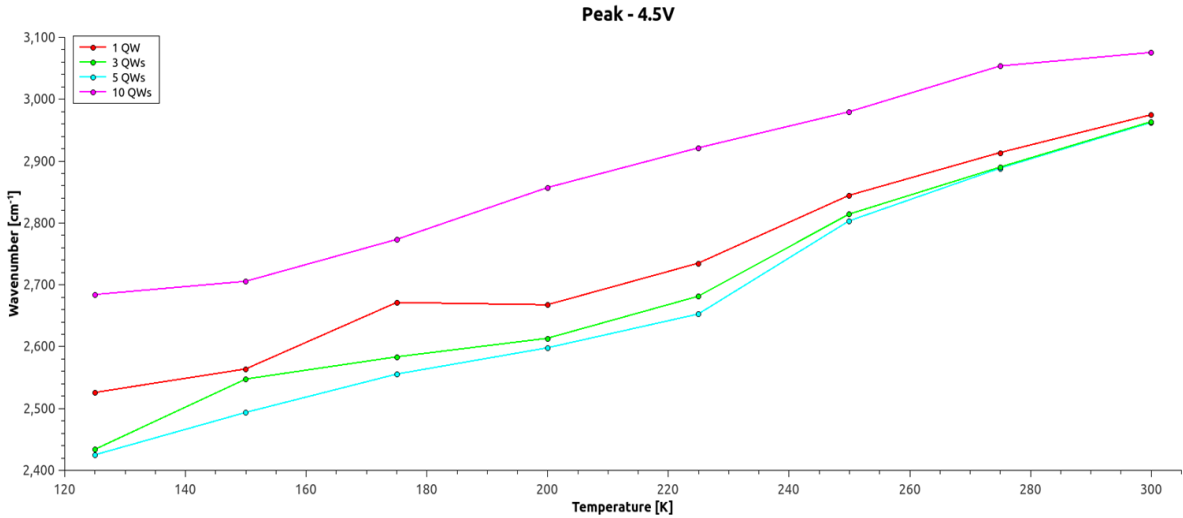


Fig. 6.21. Energies at 4.50V.

The highest energy was achieved for 10 QWs then for 1, 3 and 5. Such a huge difference in energy might have been caused by higher content of Sr in 10 QWs sample (around 2% higher than in other 3 samples).

6.3. Sr Content

To produce lasers at $3.1\mu\text{m}$, the Sr content on the barrier should be increased. In order to analyze the effect of increment of Sr in the MQW system, following experiment was performed. Three samples were measured with different Sr content.

Experimental Conditions	
Pressure	10E-4 - 10E-3
Pump Laser	$1.55\mu\text{m}$
Chopper Frequency	3800Hz
LIA Sensitivity	20mV, 50mV, 100mV
Power Excitation	3.50V, 4.50V
Temperature	125K, 150K, 175K, 200K, 225K, 250K, 275K, 300K

Samples 1767, 1757 and 1777 with strontium content of 7.40%, 9.90% and 10.60% respectively were measured to study Sr influence on PL. The arrangement of quantum wells and barriers were the same, namely 7+5 for QWs and 6+4 for barriers. While the thicknesses of barriers were the same for all the samples (15nm), the thicknesses of quantum wells were not exactly equal.

Sample Description			
Sample No.	1767	1757	1777
Substrate	Si(111)	Si(111)	Si(111)
Material	PbSe/PbSrSe	PbSe/PbSrSe	PbSe/PbSrSe
Strontium Content	7.40 %	9.90 %	10.60 %
Number of QWs	7+5	7+5	7+5
QW Thickness	4.7 nm	4.3 nm	4.4 nm
Barriers	6+4	6+4	6+4
Barrier Thickness	15nm	15nm	15nm

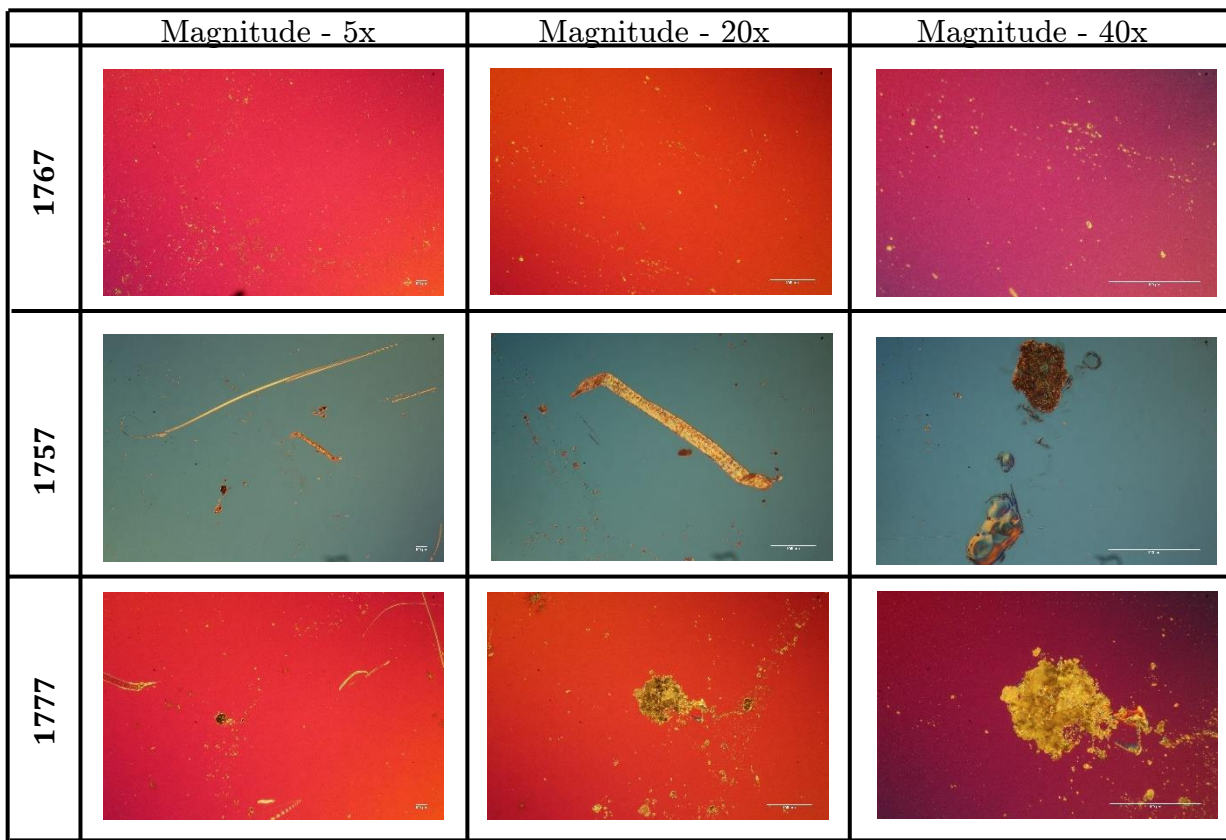


Fig. 6.22. Images of the epitaxial layers.

Sample 1767 represents a really good surface quality what cannot be said about sample 1757 where a noticeable longitudinal scratch can be pointed out. The scratch has a width of $15\mu m$ whereas a length is above $3mm$. That is a relatively big irregularity considering that the dimensions of samples are $5mm \times 5mm$. This for sure highly decreased the intensity of PL. Similar situation appears in sample 1777.

There was no PL emission for sample 1777 at power excitation $2.50V$, hence only two power excitations were taken into account. Figures below present PL spectra for $3.50V$ and $4.50V$.

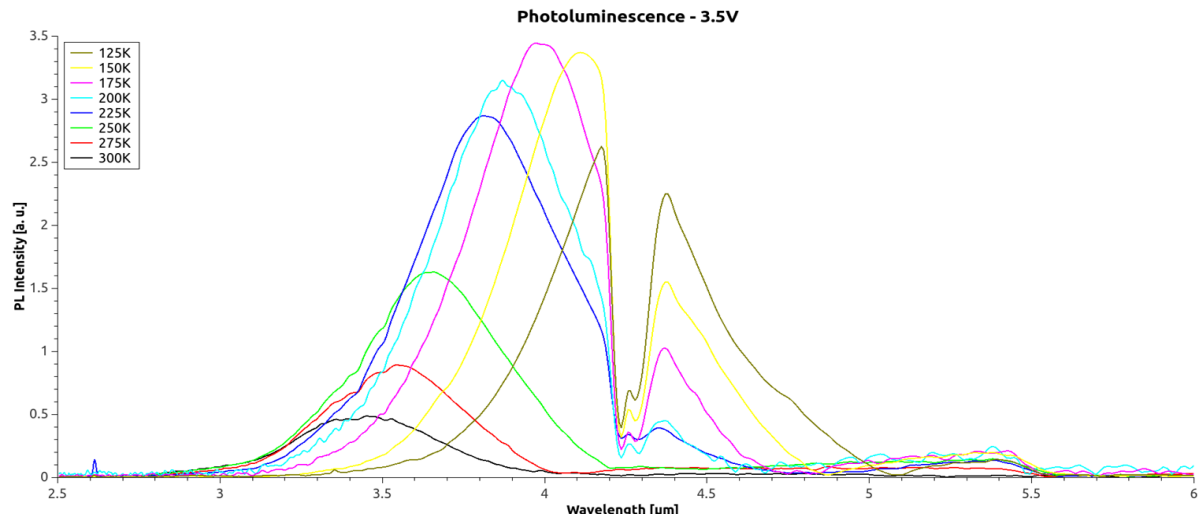


Fig. 6.23. PL spectrum at $3.50V$ - Sr 7.40%

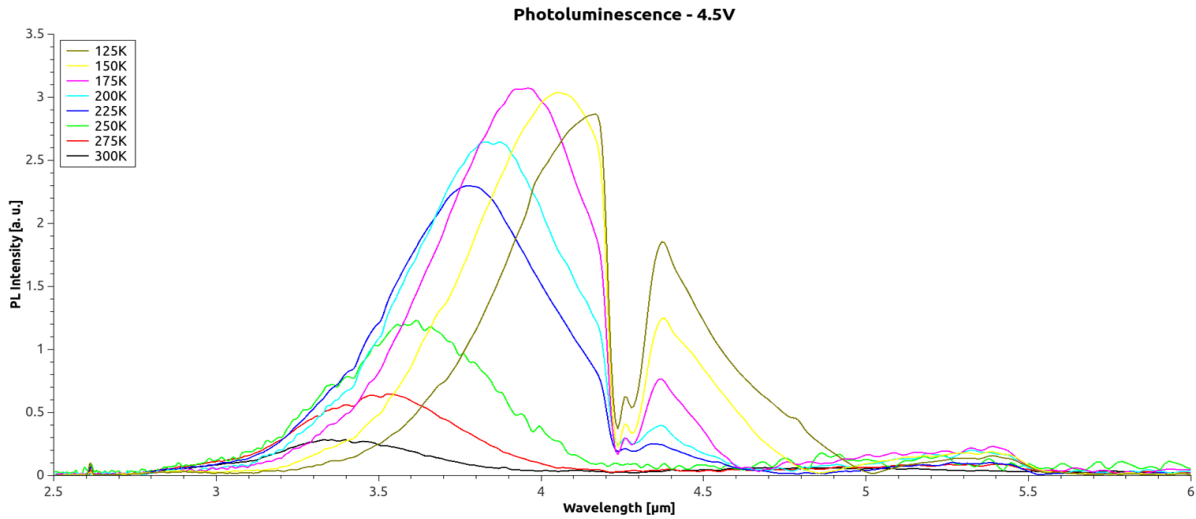


Fig. 6.24. PL spectrum at 4.50V – Sr 7.40%.

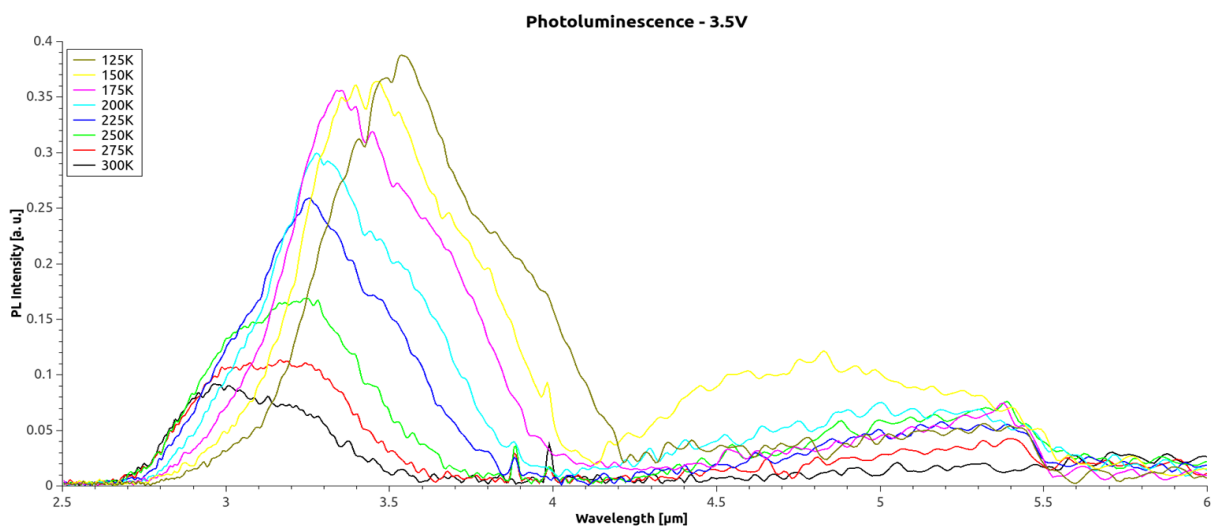


Fig. 6.25. PL spectrum at 3.50V - Sr 9.90%.

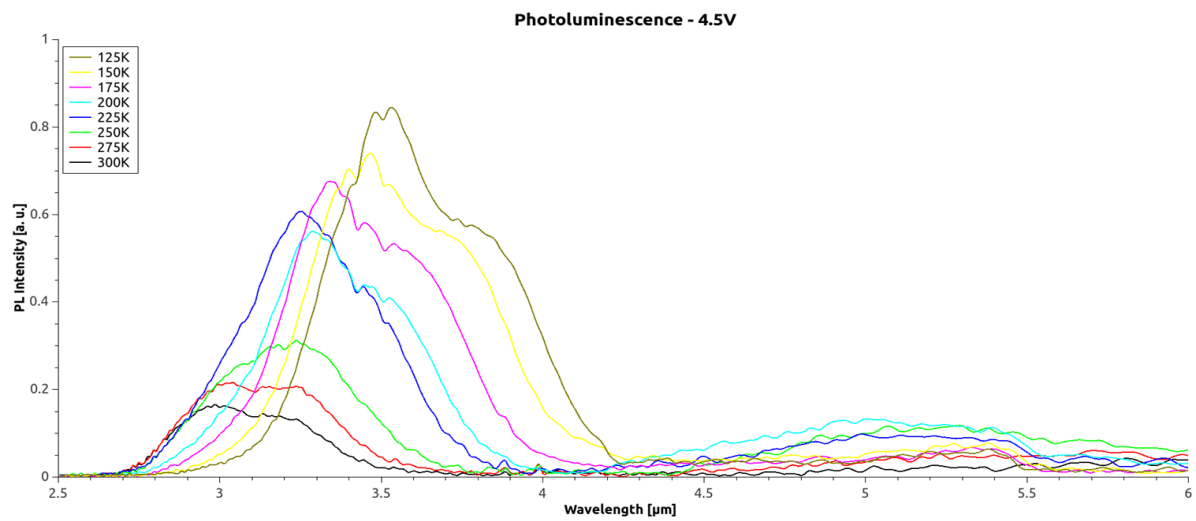


Fig. 6.26. PL spectrum at 4.50V – Sr 9.90%.

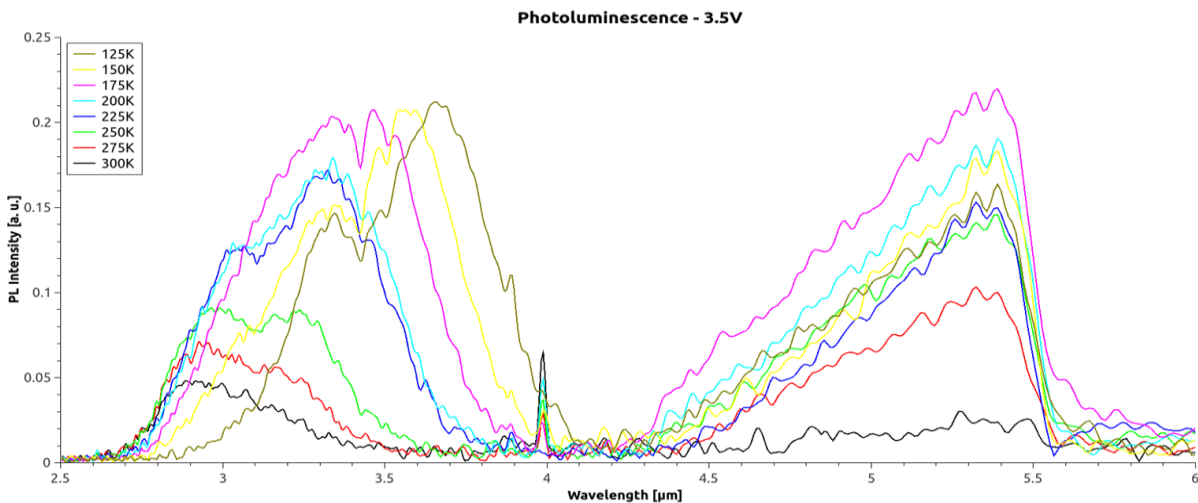


Fig. 6.27. PL spectrum at 3.50V - Sr 10.60%.

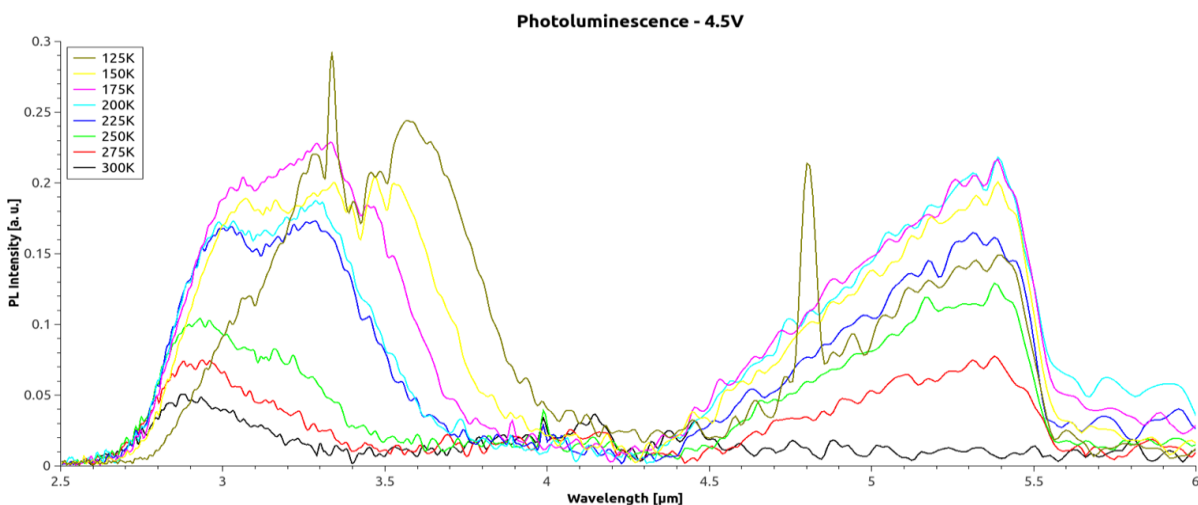


Fig. 6.28. PL spectrum at 4.50V - Sr 10.60%.

The highest intensity was achieved for sample with Sr content of 7.40%. The difference between 7.40% and 9.90%, 10.60% is distinctively higher but decreases for higher temperatures, and at the room temperature, the difference is not that huge (fig. 6.29, 6.30). The introduction of higher Sr content in the PbSrSe lattice affects the crystallographic quality of PbSrSe which results in lower PL intensity.

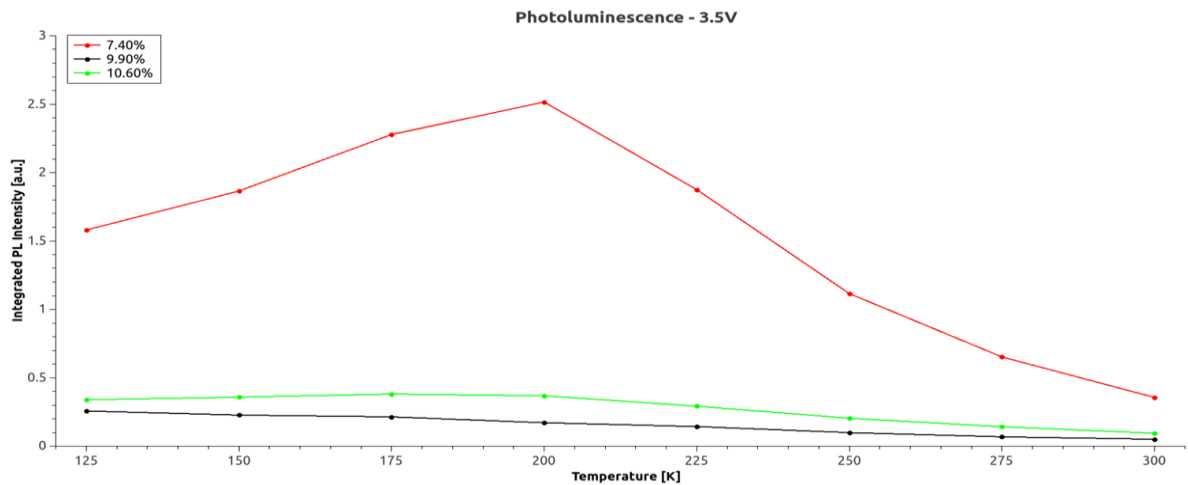


Fig. 6.29. PL intensities at 3.50V.

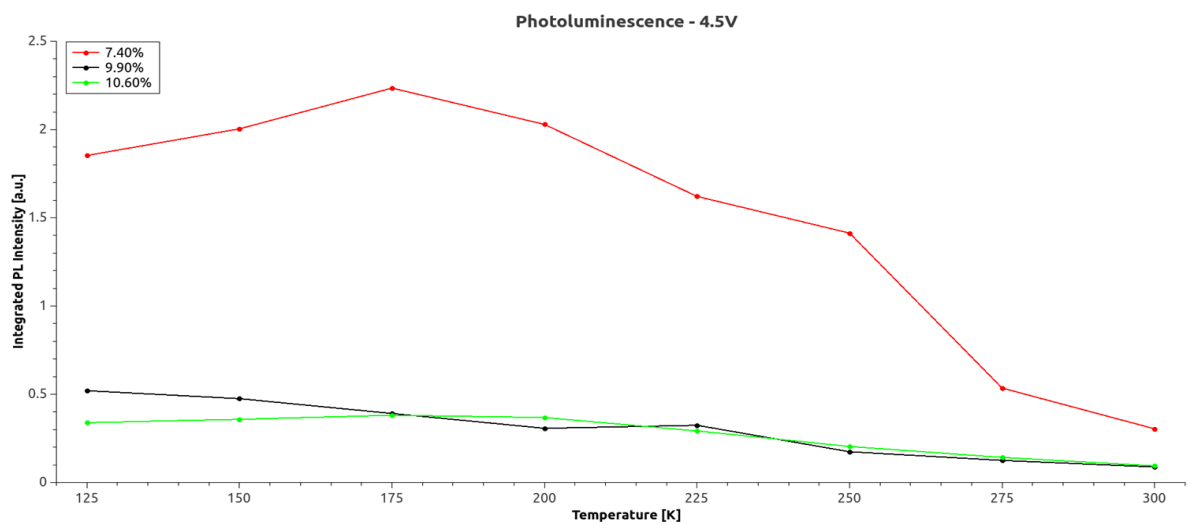


Fig. 6.30. PL intensities at 4.50V.

However, in terms of energy peak the situation is opposite. The higher the Sr content, the higher the energy, which means that Sr pushes the emission towards higher energies.

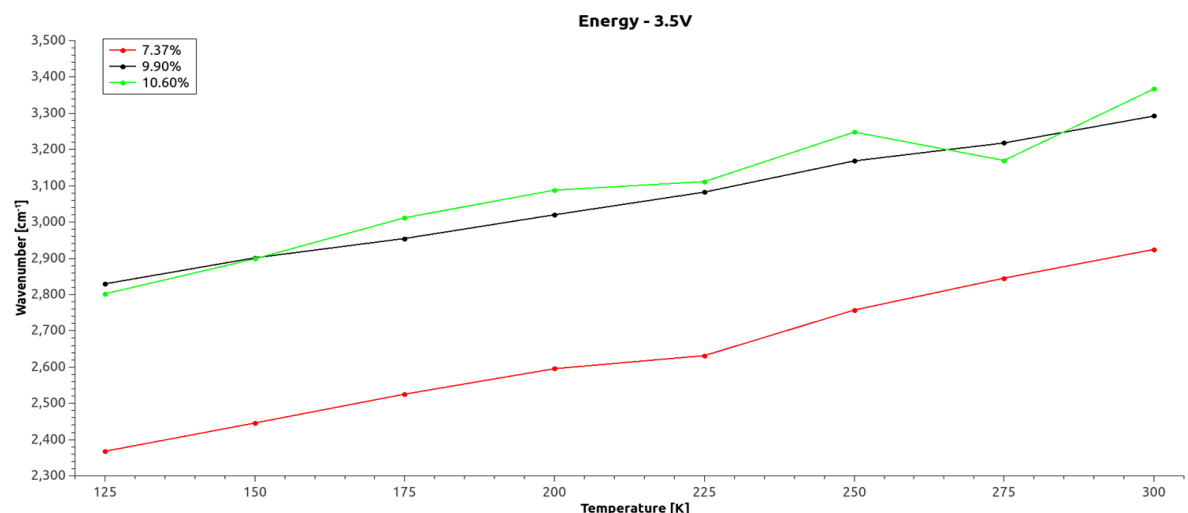


Fig. 6.31. Energies at 3.50V.

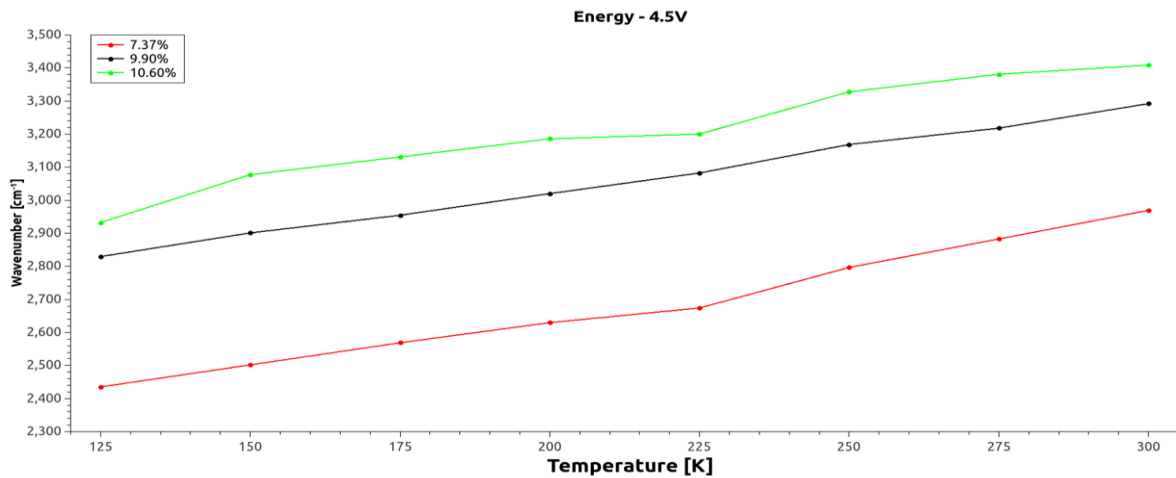


Fig. 6.32. Energies at 4.50V.

Another way to correlate temperature with PL intensity is to use so called Arrhenius plot which is given by formula:

$$I(T) = \frac{I_0 e^{\frac{-E_a}{k_B T}}}{1 + a e^{\frac{-E_a}{k_B T}}}$$

where:

$I(T)$ is the representation of integrated PL intensity at a specific temperature,

I_0 is the integrated PL intensity at $0K$,

a is the temperature dependent radiative lifetime of carriers and is a constant,

E_a is an activation energy,

k_B is a Boltzmann constant.

Arrhenius plot allows to determine critical temperature and activation energy. If we take a look at the fig. 6.29 it can be spotted, that at the $200K$ there is a steep drop. Sample with 7.40% Sr content clearly shows it. This drop in intensity happens at a specific temperature called critical temperature and is caused by thermal quenching. Thermal quenching is a decrease in efficiency of photoluminescence (in this case the intensity). If we reach critical temperature, the kinetic energy of electrons causes them to escape the quantum well and so, the recombination rate is much lower. Activation energy is the energy needed to activate thermal quenching process.

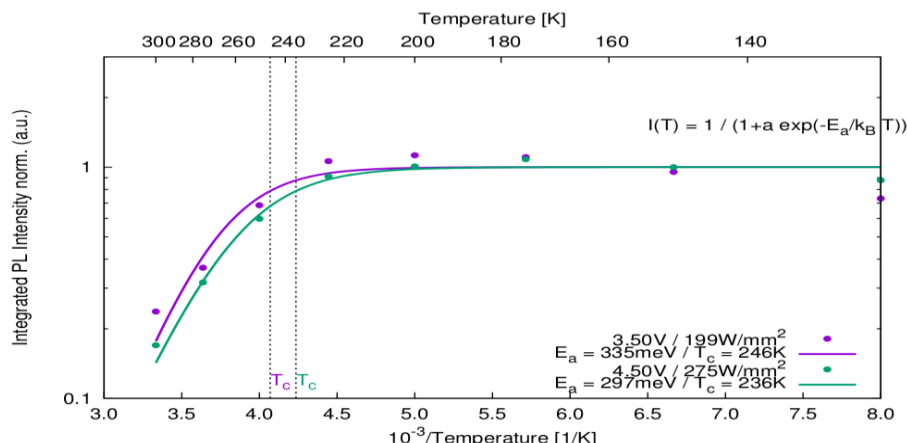


Fig. 6.33. Arrhenius plots for 3.50V and 4.50V - 7.40%.

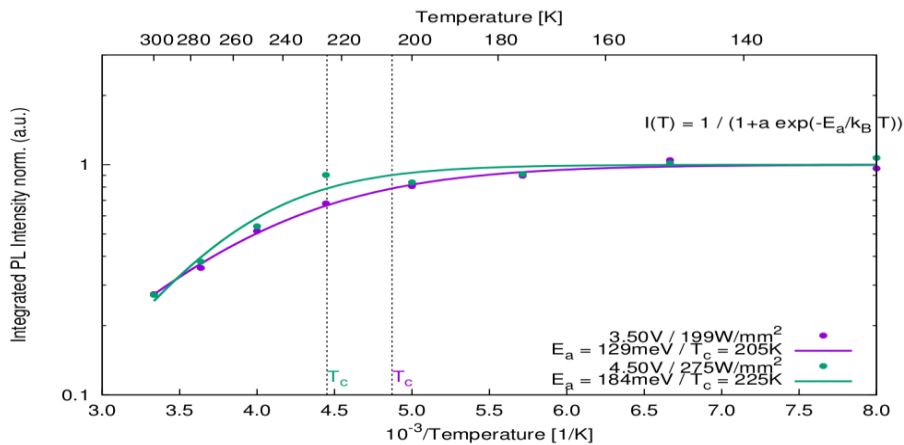


Fig. 6.34. Arrhenius plots for 3.50V and 4.50V - 9.90%.

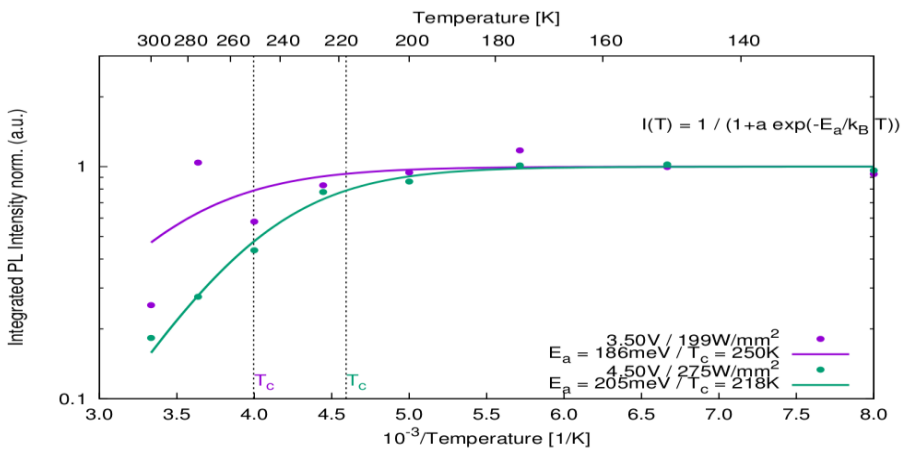


Fig. 6.35. Arrhenius plots for 3.50V and 4.50V - 10.60%.

Exc. Power Sr Content	3.50V		4.50V	
	Activation Energy	Critical Temperature	Activation Energy	Critical Temperature
7.40%	335meV	246K	297meV	246K
9.90%	128meV	205K	174meV	225K
10.60%	186meV	250K	205meV	218K

No particular trend can be indicated between Sr content and activation energy and critical temperature. At 4.50V, critical temperature tends to decrease with higher Sr content implementation but at 3.50V there is no such trend. Looking at the fig. 6.35, the curve of 3.50V is not fitted well and that might be the cause of not finding any correlations.

7. Conclusions and Final Remarks

The aim of this master thesis was to conduct photoluminescence measurements of PbSe/PbSrSe semiconductor samples with multiple quantum wells to investigate certain properties of this IV-VI semiconductor material.

The first experiment allowed to determine the accuracy (reproducibility) of the optical set-up which has been used throughout all measurements. Theoretically, different measurements of the same sample should yield exactly same results but as we know there are some factors that have an impact in some degree on conducted measurements (changes in temperature, pressure, alignment etc.). This experiment had a goal to quantify the accuracy of given optical set-up. And so, three different measurements were performed on the same sample and their results compared in terms of PL intensity and energy. Standard errors and standard deviations were calculated. As a final outcome:

- in terms of photoluminescence intensity, the accuracy is around 95.32%,
- in terms of energy, the accuracy is around 99.48%.

As a final verdict, it can be said that the set-up is highly accurate and repeatable. The deviation is caused by environmental changes and human errors, namely - additional scratching during the mounting procedure.

The purpose of the second experiment was to study dependences of quantum wells number in PbSe/PbSrSe samples. All samples provided for this master thesis were grown by MBE method. The uniformity of semiconductor quantum well stacks grown by this method are not exactly the same. The Full Width at Half Maximum was determined and plotted to find out on what scale the uniformity changes. For samples with 1, 3 and 5 quantum wells, the width was comparable, however for 10 quantum wells the difference was significant. It is caused because PL spectra of neighboring quantum wells are overlapping. The higher the number of quantum wells, the higher the intensity of photoluminescence. However, this tendency decreases while the temperature increases and is caused by thermal quenching which happens at a specific temperature called critical temperature when enough energy is delivered to activate the process. This proves theoretical considerations that if electrons are heated to a certain level, then these carriers possess enough kinetic energy to be able to escape the quantum well resulting the lower photoluminescence rate electron-hole recombination and so it may be concluded that for room temperatures, the multiple quantum wells systems are not efficient.

The last experiment was performed to analyze the effect of different strontium contents on PbSe/PbSrSe multiple quantum well systems. The highest intensity was achieved for the sample with lowest amount of strontium content whereas for the sample with highest amount of strontium content the PL intensity was the lowest. It is caused because strontium changes the lattice crystography of PbSrSe and so lowers the intensity of photoluminescence. The higher the strontium content, the more changes happen in lattice crystography. However, if we consider the energy, strontium “pushes” the emission towards higher energies.

8. Bibliography

Literature:

- [1] Ivan Pelant & Jan Valenta: Luminescence Spectroscopy of Semiconductors, OXFORD, 2012.
- [2] Anna Wojcik-Jedlinska, Kamil Pierscinski, Agata Jasik, Jan Muszalski, Maciej Bugajski: Optical Characterisation of Vertical-External-Cavity-Surface-Emitting Lasers (VECSELs), Institute of Electron Technology, Warsaw, Poland, 2007.
- [3] X. M. Fang, K. Namjou, I-Na Chao, P. J. McCann, N. Dai, G. Tor: Molecular Beam Epitaxy of PbSrSe and PbSe/PbSrSe Multiple Quantum Well Structures for Use in Midinfrared Light Emitting Devices, American Vacuum Society, 2000.
- [4] A. R. Reisinger, R. N. Roberts, S. R. Chinn, T.H. Myers II: Photoluminescence of Infrared-Sensing Materials Using a FTIR Spectrometer, American Institute of Physics, 1988.
- [5] W. Z. Shen, L.F. Jiang, K. Wang, H.Z. Wu: Spectroscopic Line Shape Broadening Mechanisms in PbSe/PbSrSe Quantum Wells, American Institute of Physics, 2002.
- [6] Y. G. Zhang, Y. Gu, K. Wang, X. Fang, A. Z. Li, K. H. Liu: Fourier Transform Infrared Spectroscopy Approach for Measurements of Photoluminescence and Electroluminescence in Mid-Infrared, American Intitute of Physics, 2012.
- [7] J. Webster: Wiley Encyklopedia of Electrical and Electronics Engineering, John Wiley & Sons, Inc., 2014.
- [8] Matthias Fill, Pierluigi Debernardi, Ferdinand Felder, Hans Zogg: Lead-Chalcogenide Mid-Infrared Vertical External Cavity Surface Emitting Lasers with Improved Treshold: Theory and Experiment, Applied Physics Letters 103, 201120, AIP Publishing LCC, 2013.
- [9] D. W. McAlister, P. J. McCann, K. Namjou, X. M. Fang, O. Alkhouri, H. Z. Wu: Midinfrared Photoluminescence from IV-VI Semiconductors Grown on Silicon, Journal of Applied Physics, Volume 89 Number 6, American Institute of Physics, 2001.
- [10] A. C. Tropper, S. Hoogland: Extended Cavity Surface-Emitting Semiconductor Lasers, Progress in Quantum Electronics, ELSEVIER, 2006.
- [11] Y. Fang, L. Wang, Q. Sun, T. Lu, Z. Deng, Z. Ma, Y. Jiang, H. Jia, W. Wang, J. Zhou, H. Chen: Investigation of Temperature-Dependent Photoluminescence in Multi-Quantum Wells, Scientific Reports, 2015.
- [12] Gunther Springholz: Molecular Beam Epitaxy and in situ Reflection High-Energy Electron Diffraction of IV-VI Semiconductor Heterostructures, Johannes Kepler-Universität Linz, 1994.

Multimedia:

- [M1] <http://www.sciencedirect.com/science/article/pii/S1369800116300579>
- [M2] <http://www.sciencedirect.com/science/article/pii/S0927025604001776>
- [M3] <https://micro.magnet.fsu.edu/primer/techniques/dic/dichome.html>